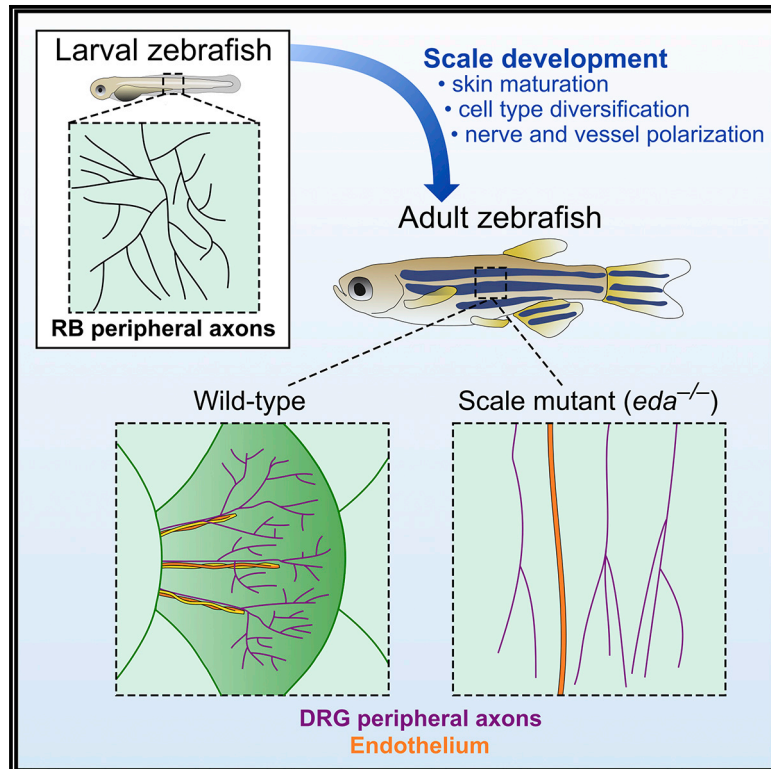


Developmental Cell

Fish Scales Dictate the Pattern of Adult Skin Innervation and Vascularization

Graphical Abstract



Authors

Jeffrey P. Rasmussen, Nhat-Thi Vo, Alvaro Sagasti

Correspondence

rasmuss@ucla.edu (J.P.R.), sagasti@mcdm.ucla.edu (A.S.)

In Brief

Rasmussen et al. show that peripheral nerves and microvasculature are patterned by bony features on fish scales. Bone-forming osteoblasts form a path on the scale surface that organizes sensory nerves and blood vessels during development, ensuring comprehensive skin innervation and vascularization.

Highlights

- Fish scale development coordinates remodeling of skin innervation and vasculature
- Scales form a guidance path for regenerating sensory nerves
- Scales promote cutaneous angiogenesis and pattern superficial capillaries
- Scales are required for nerve patterning and comprehensive innervation of the skin



Fish Scales Dictate the Pattern of Adult Skin Innervation and Vascularization

Jeffrey P. Rasmussen,^{1,*} Nhat-Thi Vo,¹ and Alvaro Sagasti^{1,2,3,*}

¹Department of Molecular, Cell and Developmental Biology, University of California, Los Angeles, CA 90095, USA

²Molecular Biology Institute, University of California, Los Angeles, CA 90095, USA

³Lead Contact

*Correspondence: rasmuss@ucla.edu (J.P.R.), sagasti@mcdb.ucla.edu (A.S.)

<https://doi.org/10.1016/j.devcel.2018.06.019>

SUMMARY

As animals mature from embryonic to adult stages, the skin grows and acquires specialized appendages, like hairs, feathers, and scales. How cutaneous blood vessels and sensory axons adapt to these dramatic changes is poorly understood. By characterizing skin maturation in zebrafish, we discovered that sensory axons are delivered to the adult epidermis in organized nerves patterned by features in bony scales. These nerves associate with blood vessels and osteoblasts above scales. Osteoblasts create paths in scales that independently guide nerves and blood vessels during both development and regeneration. By preventing scale regeneration and examining mutants lacking scales, we found that scales recruit, organize, and polarize axons and blood vessels to evenly distribute them in the skin. These studies uncover mechanisms for achieving comprehensive innervation and vascularization of the adult skin and suggest that scales coordinate a metamorphosis-like transformation of the skin with sensory axon and vascular remodeling.

INTRODUCTION

The vertebrate skin undergoes dramatic changes as animals develop from embryonic to adult stages. The epidermis grows from a simple mono- or bilayered epithelium to a stratified multi-layer epithelium, dermal vasculature elaborates, specialized sensory structures and dermal appendages appear, and the skin area greatly expands (Jenkins and Lumpkin, 2017; Johnson and Holbrook, 1989; Munger and Ide, 1988). How these events are coordinated, and how nerves and blood vessels remodel to accommodate these dramatic changes in the skin, has not been well characterized.

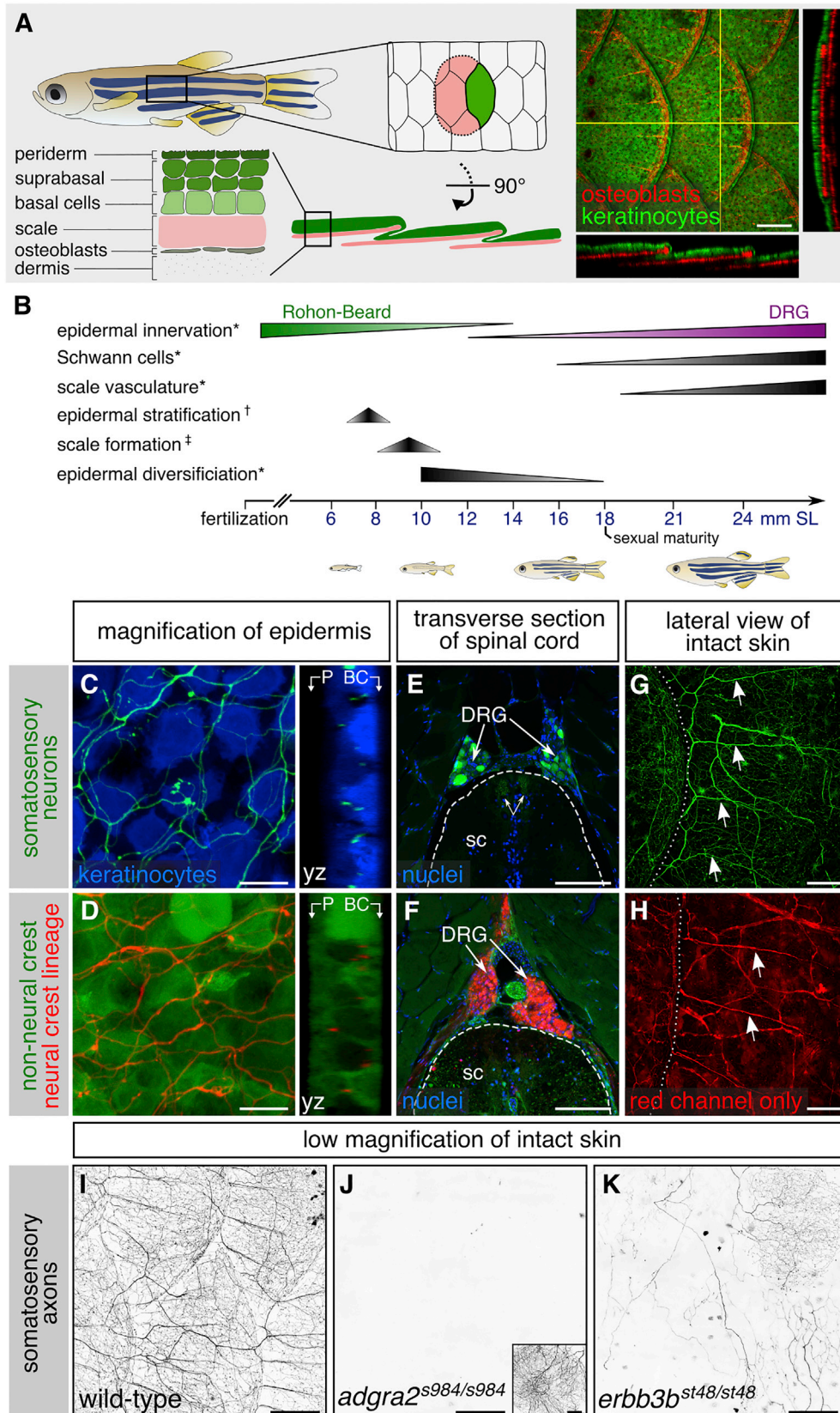
The peripheral axons of somatosensory neurons distribute their endings throughout the skin to allow animals to sense touch and avoid noxious stimuli (Jenkins and Lumpkin, 2017). Much of our understanding of somatosensory peripheral axon organization comes from studies of early development (Grueber and Sagasti, 2010; Wang et al., 2013), but adult sensory neurons likely use different mechanisms to distribute innervation across the

larger and more complex adult skin. In fish and amphibians, different neuronal populations innervate the trunk epidermis of embryos and adults. Rohon-Beard (RB) neurons in the spinal cord project peripheral axons that innervate the embryonic and larval skin, but these neurons eventually die. By contrast, adult skin is innervated by neural crest (NC)-derived dorsal root ganglion (DRG) neurons. In frogs, this RB to DRG transition occurs during metamorphosis (Hughes, 1957; Kollros and Bovbjerg, 1997; Lamborghini, 1987), but its timing in zebrafish is controversial (Cole and Ross, 2001; O'Brien et al., 2012; Palanca et al., 2013; Patten et al., 2007; Reyes et al., 2004; Slatter et al., 2005; Svoboda et al., 2001; Williams et al., 2000). The organization of peripheral axons of RB and DRG neurons fundamentally differs: RB peripheral axons do not form nerves, but rather project directly to the skin (O'Brien et al., 2012); DRG peripheral axons form nerve bundles with ensheathing Schwann cells, and associate with blood vessels (Mukouyama et al., 2002) as they project much longer distances to the skin.

Skin maturation in vertebrates is often accompanied by the appearance of dermal appendages, such as mammalian hair follicles, bird feathers, and fish scales. Despite their diverse forms, these structures are developmentally related, arising from dermal placodes that rely on the conserved ectodysplasin signaling pathway (Aman et al., 2018; Harris et al., 2008; Kondo et al., 2001; Sadier et al., 2014). Teleost fish, including zebrafish, acquire cycloid scales, mineralized bony plates that separate the dermis from the epidermis, and are arranged along the trunk in an overlapping, shingle-like pattern (Figure 1A) (Sire and Akiyenko, 2004). Zebrafish scales form at ~1–2 months of age, as fish transition from juvenile to adult forms (Figure 1B) (Parichy et al., 2009; Sire et al., 1997a; Waterman, 1970). Associations between fish scales and somatosensory nerves have not previously been reported, but bones and nerves interact in other contexts. For example, cranial nerves signal to bone-forming osteoblasts during development to create foramina, tunnels through the skull that serve as conduits to the periphery (Akbarieian et al., 2015). Sensory neurons similar to cutaneous pain-sensing neurons profusely innervate long bones (Nencini and Ivanusic, 2016) as well as diverse, specialized bony dermal appendages, such as teeth, tusks, and antlers (Hildebrand et al., 1995; Weisengruber et al., 2005; Wislocki and Singer, 1946).

How cutaneous axons and vasculature accommodate the appearance of fish scales in the skin has not been described. Here we report the discovery that scales coordinate the transition from RB to DRG skin innervation, promote innervation and vascularization of the adult skin, and determine sensory nerve





(legend on next page)

and blood vessel polarity, organizing nerves and vessels into evenly spaced channels that ensure their uniform distribution throughout the maturing skin.

RESULTS

Innervation of the Scale Epidermis Requires the Neuregulin and Wnt Pathway Proteins *Erb3b3* and *Adgra2*

To study adult skin innervation, we first surveyed transgenes and antibodies previously reported to label larval somatosensory neurons for peripheral axon labeling in adults. We thus identified several markers that label axonal free endings in the stratified epidermis above scales (Figures 1C, 1I, and S1A–S1D) (Kucenas et al., 2006; Metcalfe et al., 1990; Palanca et al., 2013; Pan et al., 2012; Udvardia, 2008). These reporters also labeled DRG cell bodies and nerves projecting toward the periphery (Figures 1E and S1E). Examination of NC-derived cells with a previously reported transgenic lineage tracing strategy (*Tg(-28.5Sox10:Cre);Tg(ubb:GswitchR)*) (Kague et al., 2012; Mosimann et al., 2011) confirmed that the adult epidermal axons labeled by these reporters belong to DRG neurons (Figures 1D, 1F, and 1H). Notably, all of these reporters revealed that DRG axons entered adult scales in strikingly organized bundles (arrows in Figures 1G, 1H, S1A, and S1D).

To determine if adult DRG neurons innervating the skin share developmental requirements with larval DRG neurons, we examined the scale epidermis in mutants of the Wnt7 co-activator *Adgra2* (*adgra2*^{s984/s984}, hereafter *adgra2*^{-/-}), and the Neuregulin receptor *Erb3b3* (*erbb3b*^{st48/st48}, hereafter *erbb3b*^{-/-}) (Lyons et al., 2005; Vanhollebeke et al., 2015), which are required for larval DRG neurogenesis and NC migration, respectively (Bostaille et al., 2017; Honjo et al., 2008; Malmquist et al., 2013; Vanhollebeke et al., 2015). *erbb3b* mutants have also been reported to lack innervation of the adult trunk (Honjo et al., 2011). In *adgra2*^{-/-} adults, the expression of a reporter for nociceptive (pain-sensing) neurons (*Tg(p2rx3a>mCherry)*) (Palanca et al., 2013) was completely absent from the trunk epidermis (Figure 1J). However, staining isolated scales for acetylated tubulin (acTubulin), which detects all axons, and examining the NC lineage reporter, revealed that *adgra2*^{-/-} scales are consistently innervated by a few NC-derived neurons that innervate basal strata of the epidermis (Figures S2K–S2O). In *erbb3b*^{-/-} adults, most scales

completely lacked innervation, as verified by acTubulin staining, but some DRG neurons were spared at all stages and innervated a few scales sparsely in adults (Figures 1K and S2A–S2J). These results indicate that, as in larvae, *Erb3b3* and *Adgra2* are required for the development of most skin-innervating adult DRG neurons, and *Adgra2* is required for all *p2rx3a* expression in DRG neurons.

A Transition in Skin Innervation Coincides with Scale Formation

Since the axon bundles we noted in adult scales are not present in larvae, we reasoned that their appearance may reflect remodeling of skin innervation. To determine when these bundles first appear, we examined skin innervation during the transition from juvenile to adult forms, spanning the 12–18 mm standard length (SL) stages, a period of rapid scale growth (Figures 1B, 2A, and 2B). The innervation pattern changed dramatically between 14 and 16 mm SL (Figure 2C). In contrast to the sparse, disorganized innervation at 12 mm SL, in scales isolated from older animals, axons were organized into regularly spaced bundles above the scale (Figure 2C'), suggesting that remodeling of skin innervation coincides with scale development.

To determine if the appearance of axon bundles correlates with the transition from RB to DRG skin innervation, we took complementary approaches to determine when RB innervation disappears and DRG innervation appears. To characterize when RB innervation is lost, we examined scales isolated from *erbb3b*^{-/-} and *adgra2*^{-/-} animals. Since these fish have specifically reduced DRG innervation, loss of epidermal axons in these mutants likely reflects loss of RB innervation. Although the density of axon innervation in mutants and sibling fish was similar at stage 12 mm SL, innervation in *adgra2*^{-/-} and *erbb3b*^{-/-} mutants was significantly reduced at 14 and 18 mm SL, respectively (Figures 2D, 2E, and 2G). Superficial axon bundles failed to appear in mutant scales (Figures 2F and 2H). These observations suggest that RB axon innervation of the skin is lost at late juvenile stages, after scale formation has initiated, and that scale-associated axon bundles do not belong to RB neurons.

To test directly when DRG innervation of the skin begins in wild-type animals, we imaged the NC lineage trace reporter, which marks DRG but not RB neurons. Prior to 12 mm SL, this reporter was robustly expressed in DRG soma but not in

Figure 1. Adult Epidermal Innervation Requires *Erb3b3* and *Adgra2*

(A) Left, diagram of adult skin anatomy. Right, confocal projection and orthogonal views through the lateral trunk. Yellow lines, planes of orthogonal sections. In this and subsequent lateral views, posterior is to the right.
 (B) Timeline of trunk skin development with approximate timing of major morphogenetic events. See Figure S3A for timing of differentiation of club cells, a specialized cell type within the fish epidermis (Whitear, 1986). *shown in this study; †based on (Guzman et al., 2013); ‡based on (Sire et al., 1997a).
 (C and D) Projections and orthogonal views through the epidermis of isolated scales. P, periderm; BC, basal cells.
 (E and F) Transverse sections through the mid-trunk. In this region, DRGs are located dorsal to the spinal cord (Weis, 1968). Double-headed arrows, DRG central axons within the spinal cord (sc). Dashed lines, spinal cord boundary.
 (G and H) Lateral views of intact adult trunk skin. Dashed lines, scale margins. Arrows, superficial axon bundles above scales.
 (I–K) Representative images of lateral trunk skin from adults of indicated genotypes. Inset in (J), trigeminal sensory axons over the eye to confirm presence of transgene.
 Transgenes: (A) keratinocytes (*Tg(krt4:EGFP)*) (Rasmussen et al., 2015) and osteoblasts (*Tg(sp7:mCherry-nfsB)*) (Singh et al., 2012); (C) keratinocytes (*Tg(actb2:BswitchR)*) (Kobayashi et al., 2014); (C, E, and G) and somatosensory neurons (*Tg(p2rx3b:EGFP)*) (Kucenas et al., 2006); (D, F, and H) *Tg(-28.5Sox10:Cre);Tg(ubb:GswitchR)* (Kague et al., 2012; Mosimann et al., 2011); (I–K) somatosensory axons (*Tg(p2rx3a>mCherry)*) (Palanca et al., 2013). Staining: (E and F) nuclei (DAPI). Scale bars, 100 μ m (A and E–H), 10 μ m (C and D), and 250 μ m (I–K). See also Figures S1 and S2.

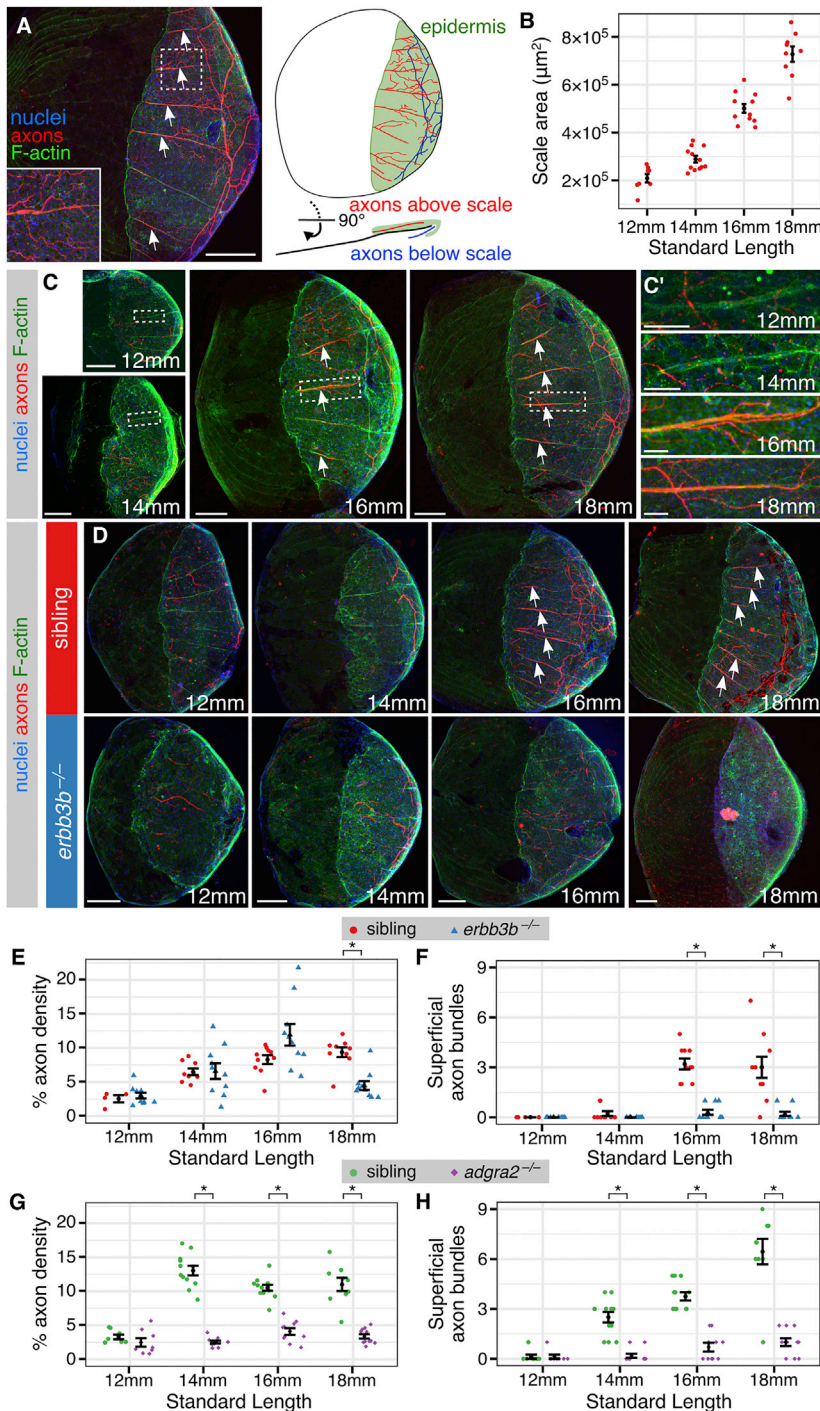


Figure 2. Remodeling of Skin Innervation during Juvenile Development

(A) Adult scale removed from animal and immunostained for indicated structures. Note that the posterior region is covered by epidermis (green).

(B) Measurements of scale size during late juvenile stages. $n = 8-12$ scales/stage. Black bars, mean \pm SEM. (C) Representative scales from juvenile animals immunostained at the indicated stages. Magnifications of epidermis are shown in **C'**. Note that elongated tracts form before nerves enter the scale.

(D) Representative scales from juvenile *erbb3b*^{-/-} and sibling controls. Note that in *erbb3b*^{-/-} scales axon bundles never form, and innervation is lost by 18 mm SL. Arrows in (**A**), (**C**) and (**D**) indicate superficial axon bundles.

(E-H) Quantification of axon density near the skin (**E** and **G**) and superficial axon bundles (**F** and **H**) based on acTubulin staining. $n = 4-12$ scales/sample (mean sample size = 9.7). Black bars, mean \pm SEM. * $p < 0.01$, Wilcoxon rank-sum test.

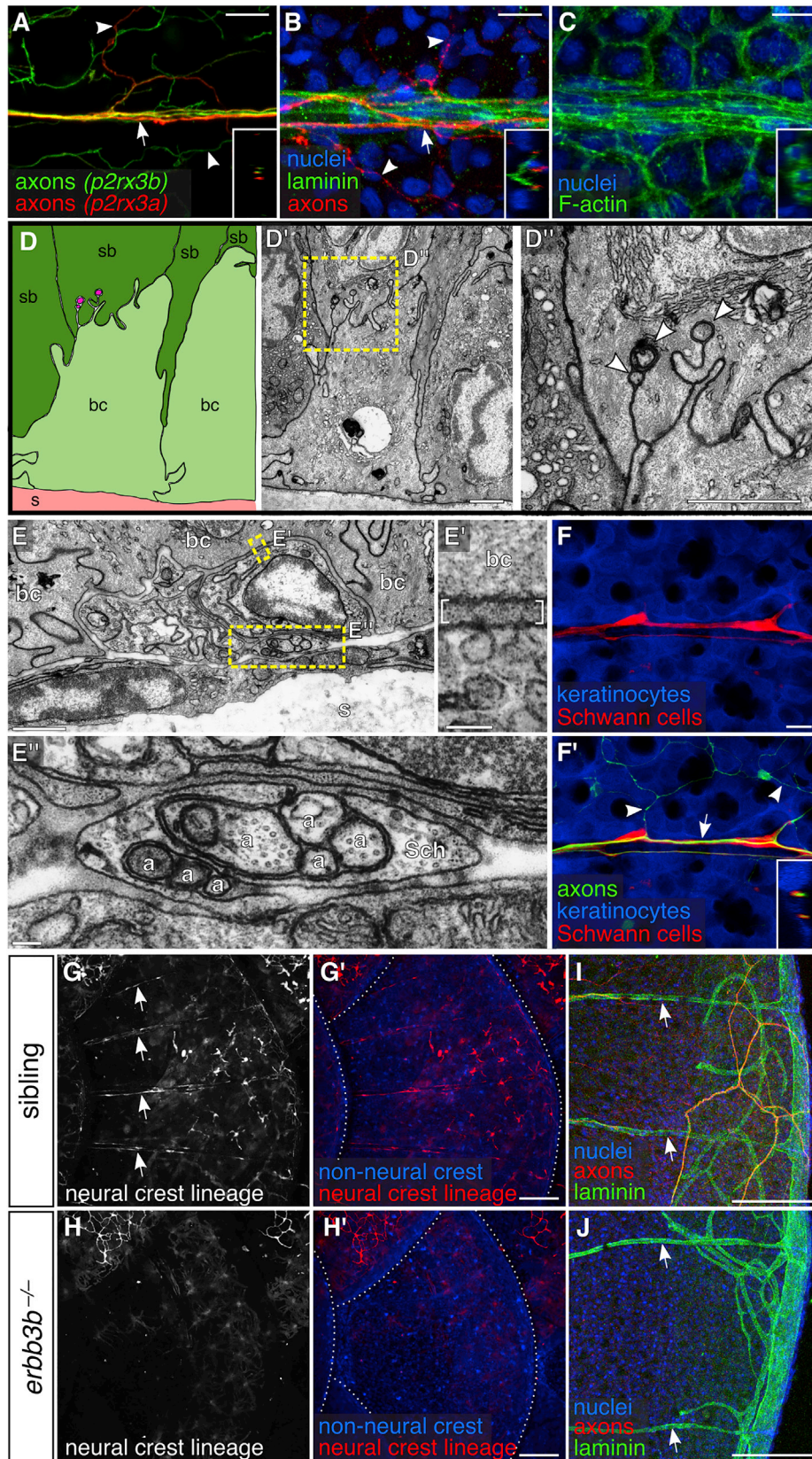
Staining: (**A**, **C**, and **D**) F-actin (phalloidin), axons (acTubulin) and nuclei (DAPI). Scale bars, 250 μ m (**A**), 100 μ m (**C** and **D**), and 25 μ m (**C'**). See also [Figure S3](#).

DRG Nerves Occupy Extracellular Matrix-Rich Tracts on the Surface of Scales that Form Independent of Neurons and Glia

To determine if scale-associated DRG axon bundles display hallmarks of peripheral nerves, we stained scales for the extracellular matrix (ECM) component laminin and examined markers of Schwann cells. As expected, laminin was associated with sensory axon bundles, but not with free endings in the epidermis ([Figures 3A](#) and [3B](#)), and was concentrated along the interface between the bundles and epidermis ([Figure 3B](#), inset). We identified a combination of previously described transgenic lines for NC lineage tracing (*Tg(-28.5Sox10:Cre);Tg(actb2:BswitchR)*) ([Kague et al., 2012](#); [Kobayashi et al., 2014](#)) that marked elongated cells resembling Schwann cells but was only weakly expressed in sensory axons themselves ([Figures 3C](#) and [3F](#)). These cells were intimately associated with axons, as expected for Schwann cells ([Figure 3F'](#)), and migrated in tight association with axon bundles as they entered scales ([Figure S3C](#)). To confirm these

observations, we performed transmission electron microscopy (TEM) on scales isolated from adult zebrafish. Within the epidermis, we identified individual axons with diameters similar to nociceptive axon free endings (area = $0.022 \pm 0.015 \mu\text{m}^2$; mean \pm SD; $n = 23$), which were not obviously associated with ECM but were frequently ensheathed by keratinocytes ([Figure 3D](#)), similar to RB peripheral axons in larval zebrafish ([O'Brien et al., 2012](#)). Below the epidermis, but above the mineralized scale, axons formed periodic bundles that were ensheathed by

axons innervating the epidermis ([Figures S3A](#) and [S3B](#)). At ~ 14 mm SL, DRG axons began extending along the scale surface in an anterior-to-posterior direction (arrowheads in [Figure S3A](#)). These observations indicate that DRG axons innervate the scale epidermis as RBs are disappearing. Furthermore, pathfinding DRG axons are organized in bundles along the scale surface, suggesting that they may form scale-associated nerves, which have not been previously described.



(legend on next page)

nonmyelinating Schwann cells (Figures 3E and 3E''). Electron dense extracellular material separated these axon bundles and several other cell types from basal keratinocytes (Figure 3E').

To determine if Schwann cells create the nerve-associated ECM, as they do in other peripheral nerves (Chen and Strickland, 2003; Lentz et al., 1997; Yu et al., 2009), we stained for laminin in scales of mutants lacking Schwann cells. In mammals, nonmyelinating Schwann cell development requires *ErbB3* signaling (Chen et al., 2003; Riethmacher et al., 1997). Similarly, *erbb3b*^{-/-} adult zebrafish lacked Schwann cells (Figures 3G and 3H). Surprisingly, the laminin pattern in these mutants was indistinguishable from controls (Figures 3I and 3J), demonstrating that neither DRG neurons nor associated Schwann cells are required to produce the ECM lining superficial scale nerves.

Scales Vascularize Independent of Sensory Nerves

Since blood vessels often interact with peripheral nerves (Makita, 2013; Mukouyama et al., 2002), secrete ECM (Hallmann et al., 2005), and have been observed along the scale surface (Sire et al., 1997b), we wondered if they might create the ECM associated with nerves. By examining an endothelial reporter transgene (*Tg(fli1a:EGFP)*) (Lawson and Weinstein, 2002), we found that microvasculature formed a stereotyped pattern along the scale surface and posterior scale margin (Figure 4A, arrows and arrowheads, respectively). Vessels on the scale surface were strikingly congruent with superficial scale nerves, but dermal vasculature was not obviously associated with sensory nerves below scales (Figures 4A and 4C). Scale-associated capillaries consisted of two intertwined vessels expressing the tight junction marker *Tjp1* (formerly *Zo-1*) (Figures 4C, 4D, and 4F). Similar to capillary loops in human dermal papillae (Braverman and Yen, 1977), one of these vessels was arterial (Figure 4D). Lymphatic endothelium occasionally associated with these capillaries (Figure 4E).

To determine when the vascular pattern appears, we examined trunk skin during late juvenile stages. By 14 mm SL, large-caliber vessels had entered the dermis beneath each scale, but capillaries only extended along the scale surface beginning at 18–19 mm SL (Figures S4A–S4D), well after the formation of superficial scale nerves (Figure S4E). The timing of scale vascularization suggests that blood vessels neither secrete the nerve-associated ECM nor guide nerves onto scales. To test if instead nerves guide blood vessels onto scales, we examined *erbb3b*^{-/-}

and *adgra2*^{-/-} scales but found that vasculature developed normally in the absence of axons (Figures 4B and 4G–I). Thus, vascularization of the scale surface occurs after nerve formation but does not require nerves.

Scale Nerves and Capillaries Extend along Osteoblast-Lined Scale Radii

To determine if other cells, or structures associated with scales, determine the pattern of innervation or vascularization, we examined how nerves and blood vessels relate to scale features. Capillaries were previously noted along radii (Sire et al., 1997b), grooves in the mineralized surface that radiate from an anterior focus to the posterior scale margin (Sire et al., 1997b; Waterman, 1970). Superficial scale nerves and capillaries were remarkably congruent with scale radii (Figures 5A, S5A, and S5B). This congruence was maintained in scales with deviations in the normal radial orientation of the grooves (Figure 5B), in scales from aged individuals with increased numbers of radii (Figure 5C), and in scales from different regions of the body, which have distinct scale morphologies and radial spacing (Figure S6). Most radii were occupied by nerves, but only a subset of these had capillaries, demonstrating that nerves do not require associated vasculature for their maintenance (Figure S6). Together these observations suggest that radii, or cells associated with them, pattern superficial nerves and vasculature.

Bone-producing osteoblasts have been proposed to initiate radius formation (Sire et al., 1997a; Waterman, 1970), and bone-resorbing osteoclasts have been observed along radii (Sharif et al., 2014; de Vrieze et al., 2011). Scale nerves formed normally in *csfr1a*^{i4blue/j4blue} mutants (Parichy et al., 2000) (Figure S5C), which lack most osteoclasts (Chatani et al., 2011), indicating that osteoclasts are not required for radial morphogenesis. To image mature osteoblasts, we used a previously developed transgenic reporter (*Tg(sp7:mCherry-nfsB)*) and the antibody zns-5 (Johnson and Weston, 1995; Singh et al., 2012). In addition to hyposquamal (below the scale) osteoblasts, we found that episquamal (above the scale) osteoblasts formed chains running along radii, tightly associated with superficial scale nerves (Figures 5D, 5F, and 5G). Radial osteoblasts appeared early in scale growth (Figure 5I), consistent with previous studies (Sire et al., 1997a; Waterman, 1970), and migrated from the posterior margin toward the focus. Osteoblasts were present along radii of *erbb3b*^{-/-} adults (Figure 5H), demonstrating that they associate with radii independent of nerves.

Figure 3. DRG Axons Form Nerves at the Surface of Scales

(A–C) Projections through a single superficial scale nerve in an adult. Arrow, axon bundle. Arrowheads, axon free endings. Insets, orthogonal views of nerve; outer surface to left.

(D) TEM of scale epidermis. Arrowheads, axon free endings ensheathed by keratinocyte membranes. Yellow box, area of magnification.

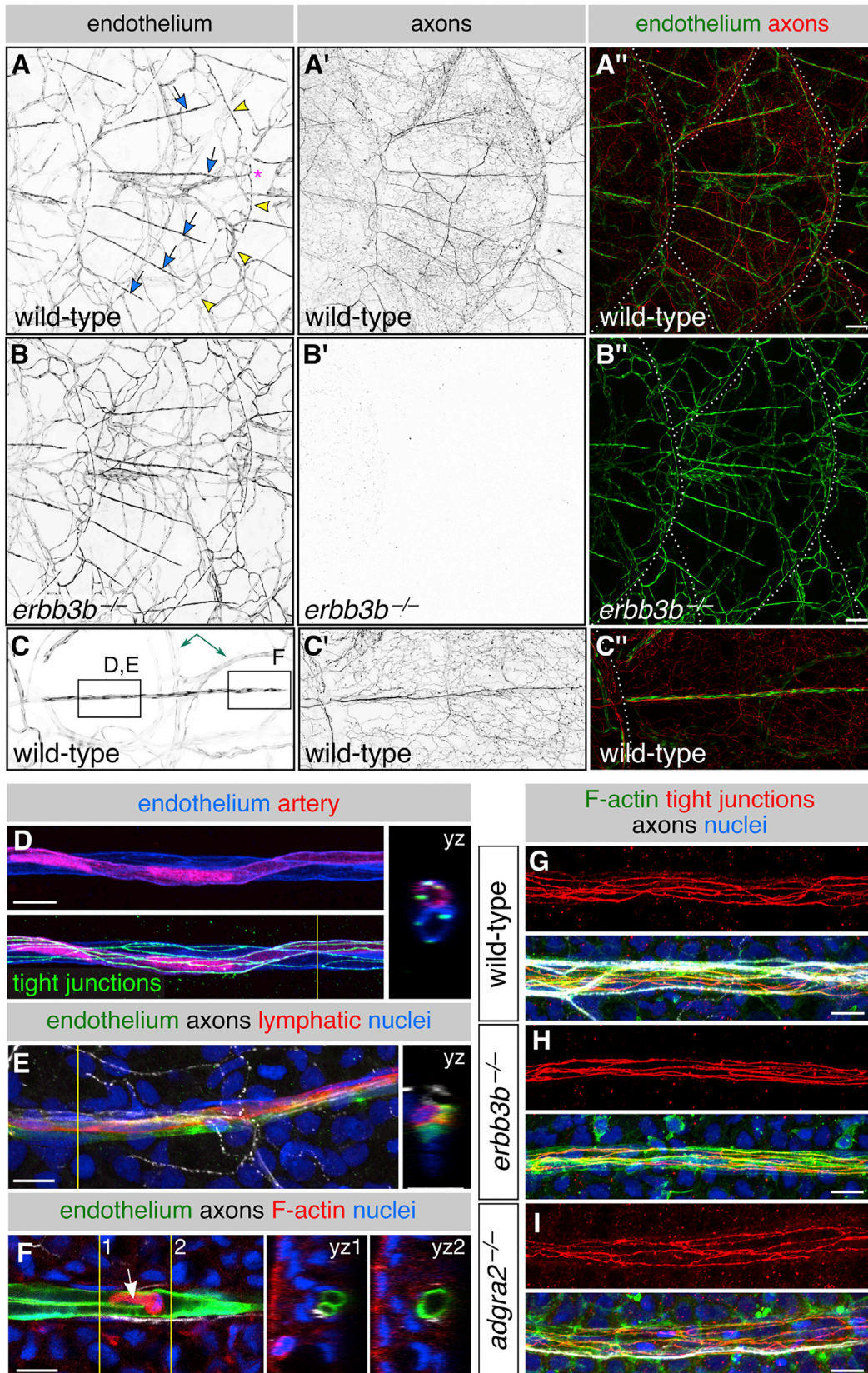
(E) Transverse TEM of superficial scale nerve. Yellow boxes, areas of magnification. Brackets in E' indicate electron dense extracellular material. a, axon; Sch, Schwann cell; bc, basal cell; sb, suprabasal cell; s, scale.

(F) DRG axons and associated Schwann cells (arrow in F') along the scale surface. Note that free endings in the epidermis (arrowheads) are not associated with Schwann cells. Inset, orthogonal view of nerve.

(G and H) Representative lateral views of the trunk of adult *erbb3b*^{-/-} and sibling controls. Arrows, scale nerve-associated Schwann cells. Dashed lines, scale margins.

(I and J) Representative scales from adult *erbb3b*^{-/-} and sibling controls immunostained for indicated markers. Arrows, superficial laminin tracts.

Transgenes: (A) *Tg(p2rx3b:EGFP)* and *Tg(p2rx3a>mCherry)* (these two transgenes label nociceptive sensory neurons, but, as in larvae, *P2rx3a* appears to label a subset of *P2rx3b* neurons; Gau et al., 2013; Palanca et al., 2013); (F) axons (*Tg(p2rx3b:EGFP)*), and keratinocytes and Schwann cells (*Tg(-28.5Sox10:Cre);Tg(actb2:BswitchR)*); (G and H) *Tg(-28.5Sox10:Cre);Tg(actb2:BswitchR)*. Staining: (B, I, and J) laminin (anti-laminin), axons (acTubulin), and nuclei (DAPI); (C) F-actin (phalloidin) and nuclei (DAPI). Scale bars, 10 μ m (A–C and F), 1 μ m (D and E), 0.1 μ m (E' and E''), and 100 μ m (G–J).



(legend on next page)

Because radial osteoblasts form prior to and independent of scale nerves, we wondered if they create the nerve-associated ECM. The laminin pattern in scales isolated prior to superficial nerve formation and vascularization closely mirrored osteoblasts (Figures S5D–S5F). Basal epidermal cells contained intracellular laminin puncta, suggesting that they secrete ECM components (Figures S5F' and S5F''). Variations from the radial pattern of laminin staining in adult scales were associated with osteoblasts (Figure 5E), consistent with the possibility that osteoblasts secrete or concentrate laminin along scale nerves.

Regenerating Axons Are Guided by Pre-existing Radial Tracts

Given the close association between radial osteoblasts and sensory nerves, and the observation that osteoblasts co-localize with ECM before nerves enter scales, we hypothesized that radii guide nerves. To test if radii can serve as a template for regenerating sensory axons, we transplanted scales between adult animals (Figure 5J). Scale removal physically severs axons, causing their degeneration and rapid clearance from the detached scale. Upon transplantation, these denervated scales were robustly re-innervated along radii by regenerating host axons (Figures 5K and 5L). Similar axon regeneration occurred along radii of scales transplanted from *erbb3b*^{+/-} and *erbb3b*^{-/-} animals (Figures 5M and 5N). Thus, radii can guide regenerating axons whether or not they were previously innervated during development.

Osteoblasts, but Not Blood Vessels, Promote Re-innervation during Regeneration

Since scale radii facilitate the entry of regenerating nerves into the epidermis, we hypothesized that scales are required for epidermal innervation. We first tested this hypothesis in the context of regeneration, since zebrafish scales robustly regenerate (Aman et al., 2018; Sire et al., 1997a, 1997b). In wild-type adults, following scale removal, scales and their associated sensory axons had significantly regenerated by 7 days post injury (dpi) (Figure 6A). The order of cell type assembly along radii during regeneration recapitulated the ontogenic sequence: osteoblasts and ECM appeared first, followed by sensory axons, then Schwann cells, and then vasculature.

To test the role of angiogenesis in scale and nerve regeneration, we induced scale regeneration in the presence of the vascular endothelial growth factor receptor (VEGFR) inhibitor, PTK787 (Figure 6B). In fish treated with this drug, scales regenerated and were re-innervated but never acquired radial vasculature (Figures 6C, 6E, and 6F), confirming that blood vessels are required neither for the formation of nerves nor to maintain

them for at least 3 weeks. Innervation density was mildly, but not significantly, reduced in the absence of angiogenesis (Figure 6D), which could be due to direct or indirect effects of the VEGFR inhibitor on axon growth.

To test if scales are required for regenerating axons to re-innervate the epidermis, we used a previously established transgenic strategy to conditionally ablate osteoblasts prior to scale removal (Figure 6G). In this approach, the nitroreductase enzyme is specifically expressed in osteoblasts (*Tg(sp7:mCherry-nfsB)*) (Singh et al., 2012). Treatment with the normally benign prodrug metronidazole (Mtz) causes cell-autonomous death of nitroreductase-expressing cells (Curado et al., 2007). Mtz treatment alone unexpectedly reduced re-innervation, but, in animals with nitroreductase-expressing osteoblasts, Mtz treatment ablated osteoblasts, prevented scale regeneration, and reduced re-innervation further (Figures 6H–6J and S5G). Thus, osteoblasts and/or scales promote skin innervation during regeneration.

Scales Locally Organize and Promote Innervation, Vascularization, and Maturation of the Skin

To determine if scales are also required during development to establish the pattern of skin innervation or vascularization, we compared axon and blood vessel organization in wild-type fish and mutants with defective scale development. In wild-type animals, nerve and blood vessel polarity was reoriented from a primarily dorsal-ventral orientation below scales to an anterior-posterior orientation above scales (Figures 7A, 7B, 7B', and 7E'; green and magenta traces in Figure 7E'', respectively). By contrast, in ectodysplasin A (*eda*^{nkt/nkt}) mutant animals, which completely lack scales (Figure 7C) (Harris et al., 2008), nerves and blood vessels were oriented primarily in a dorsal-ventral orientation (Figures 7D, 7D', S7A, and S7C). In fibroblast growth factor receptor 1a (*fgfr1a*^{spd/spd}) mutants, which have reduced numbers of scales (Rohner et al., 2009), we occasionally found scales with reversed orientation: scales emerged from posterior to anterior, rather than the wild-type anterior-to-posterior pattern (Figures 7E and 7F). Within these reversed scales, the polarity of sensory axons was similarly inverted, demonstrating that scales dictate the axis of sensory innervation of the epidermis (Figures 7F'–7F'').

Examining *eda* mutants revealed that, in addition to orienting nerves and blood vessels, scales promote vascularization, innervation, and skin maturation. The density of blood vessels near the skin was severely reduced in *eda*^{nkt/nkt} mutants, indicating that scales not only induce the formation of capillaries above scales but also promote dermal angiogenesis below scales

Figure 4. Scales Vascularize Independently of Sensory Axons

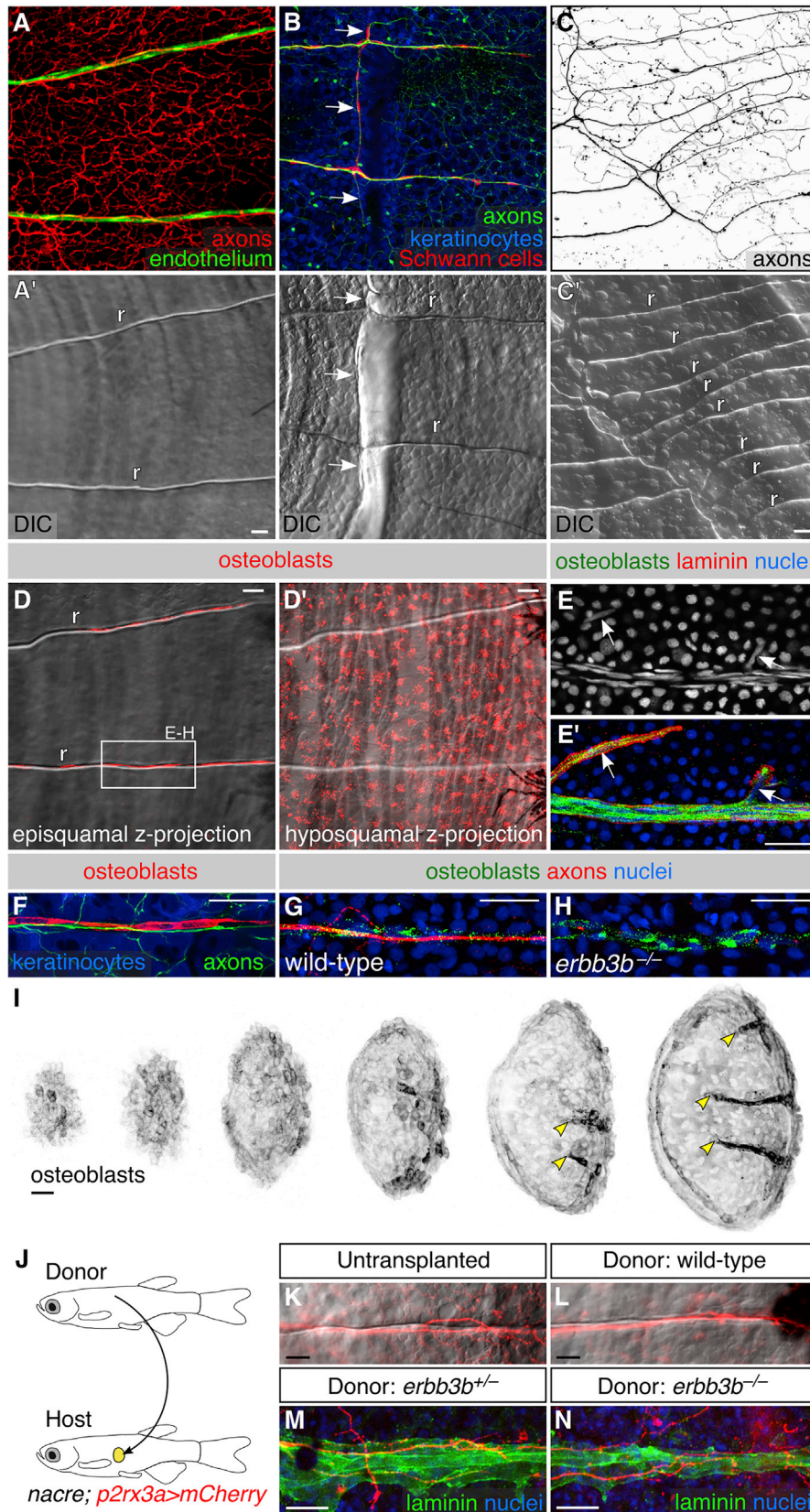
(A–C) Representative lateral views of the trunk from wild-type and *erbb3b*^{-/-} adults. Arrows, superficial scale capillaries. Arrowheads, microvasculature associated with scale margin. Asterisk, interconnection of superficial capillary with scale margin vasculature. Dashed lines, scale margins. Double-headed arrow, example of dermal vasculature not associated with sensory nerves. Boxes in (C) indicate areas of magnification for (D)–(F).

(D and E) Magnification of scale capillaries. Note the two intertwined vessels in (D).

(F) Single z section through the tip of a scale capillary. Orthogonal views show that vessel lumens merge near posterior tip to form a U shape. Arrow, cell within the vessel lumen. Yellow lines in (D)–(F), planes of orthogonal sections.

(G–I) Representative scale capillaries immunostained for the indicated markers from adult wild-type, *erbb3b*^{-/-} and *adgra2*^{-/-} fish.

Transgenes: endothelium (*Tg(fli1a:EGFP)*); (A–C) axons (*Tg(p2rx3a>mCherry)*); (D) artery (*Tg(-0.8ftt1:RFP)*) (Bussmann et al., 2010); lymphatic (*TgBAC(prox1a:KALTA4,4xUAS-ADV.E1b:TagRFP)*) (van Impel et al., 2014). Staining: (D) tight junctions (anti-Tjp1); (E) axons (acTubulin) and nuclei (DAPI); (F) F-actin (phalloidin), axons (acTubulin), and nuclei (DAPI); (G–I) F-actin (phalloidin), tight junctions (anti-Tjp1), axons (acTubulin), and nuclei (DAPI). Scale bars, 100 μ m (A–C) and 10 μ m (D–I). See also Figure S4.



(legend on next page)

(Figures 7B', 7D', and S7B). Fine-caliber axons characteristic of epidermal free ending were also reduced in *eda^{nkt/nkt}* mutant skin (insets in Figures 7B and 7D), suggesting that scales target axons to the epidermis during development. Unexpectedly, the epidermis in these mutants lacked specialized features of adult skin, such as club cells, which release alarm signals in damaged skin, and breeding tubercles, male-specific, keratin-rich structures (Figures S7D and S7E and data not shown) (Whitewar, 1986; Wiley and Collette, 1970), indicating that scales are also required for maturation of the skin.

To determine if signals from scales act locally or systemically to regulate innervation, vascularization, or skin maturation, we compared regions of non-squamated ("naked") skin with regions of squamated skin in *fgfr1a^{spd/spd}* mutants and heterozygous *eda* mutants (*eda^{nkt/+}*), both of which lack some scales (Harris et al., 2008; Rohner et al., 2009), resulting in fish with patches of naked skin interspersed among squamated skin (Figures 7G and 7H). Naked skin regions in both mutants had a dramatically lower density of epidermal sensory endings than neighboring squamated skin (Figures 7G–7I). Naked skin was also thinner and lacked club cells and breeding tubercles, whereas neighboring squamated skin was stratified and contained abundant club cells and breeding tubercles (Figures 7H' and S7F–S7J). Thus, scales signal locally to promote innervation, stratification, and the development of specialized cell types in the skin.

DISCUSSION

As embryos develop from embryonic to juvenile and adult forms, the skin undergoes dramatic growth and remodeling, requiring concomitant reorganization of the cutaneous blood vessels and sensory endings mediating touch (Jenkins and Lumpkin, 2017). We report that, in zebrafish, a transition in skin innervation from RB to DRG neurons, is coordinated with the formation of bony scales. DRG peripheral axons are organized into nerves that associate with blood vessels along scale features called radii. Bone-forming osteoblasts pioneer these radial tracts, which independently guide both

innervation and vascularization. Our findings uncover roles for scales in promoting and polarizing skin innervation and vascularization, and organizing nerves and blood vessels into regularly spaced patterns, thus ensuring their even distribution in the skin.

Sensory Remodeling Is Coordinated with Skin Maturation

We found that the loss of RB neurons, and the appearance of DRG sensory endings in the epidermis, occurs much later than previously thought; several weeks into development rather than a few days. Reports of early RB loss may reflect the loss of antigen or transgene expression used to observe them, or death of a minor subset of RB neurons, with many persisting until the onset of metamorphosis, similar to frogs (Kollros and Bovbjerg, 1997). Although the perception that RB neurons die during the first week of development persists, our results are consistent with reports indicating that RB neurons survive for weeks (O'Brien et al., 2012; Palanca et al., 2013; Patten et al., 2007; Reyes et al., 2004; Slatter et al., 2005).

Our findings place the remodeling of skin innervation coincident with scale development and stratification of the epidermal epithelium. This apparent correspondence between the remodeling of skin and sensory endings is similar in other animals, like insects and amphibians, in which these metamorphic events are hormonally coordinated (Kollros and Bovbjerg, 1997; Yaniv and Schuldiner, 2016). Scale formation, stratification, dermal vascularization, and sensory remodeling could each be independently regulated, but our results suggest that scales are required for the other processes, since the epithelium was thinner, vasculature was reduced, and innervation was sparser in naked skin regions of *fgfr1a* and *eda* mutants. Mammals do not undergo an obvious metamorphosis-like transition, but the skin undergoes dramatic growth, stratification, and cell type diversification during development. Although mammals are not widely thought to have RB neurons, similar embryonic neurons in the spinal cord have been described (Humphrey, 1944, 1947, 1950; Youngstrom, 1944), raising the possibility that mammalian skin may undergo similar sensory remodeling.

Figure 5. Neurovascular Congruence with Radial Osteoblasts.

(A–C) Fluorescent and differential interference contrast (DIC) images showing congruence between nerves and scale radii in wild-type animals. r, radius. Arrows, areas of nerve-radius congruence. In (C), the scale was from a 2-year-old, 31 mm SL fish. r, radius.

(D) Episquamal osteoblasts localize along radii.

(E) Scale nerve immunostained as indicated. Note the close apposition between osteoblasts and laminin staining. Arrows, single osteoblast nuclei.

(F) Congruence between episquamal osteoblasts and scale nerve.

(G and H) Representative scale nerves from adult wild-type and *erbb3b^{-/-}* fish immunostained for indicated markers. Note that radial osteoblasts form normally in the absence of axons.

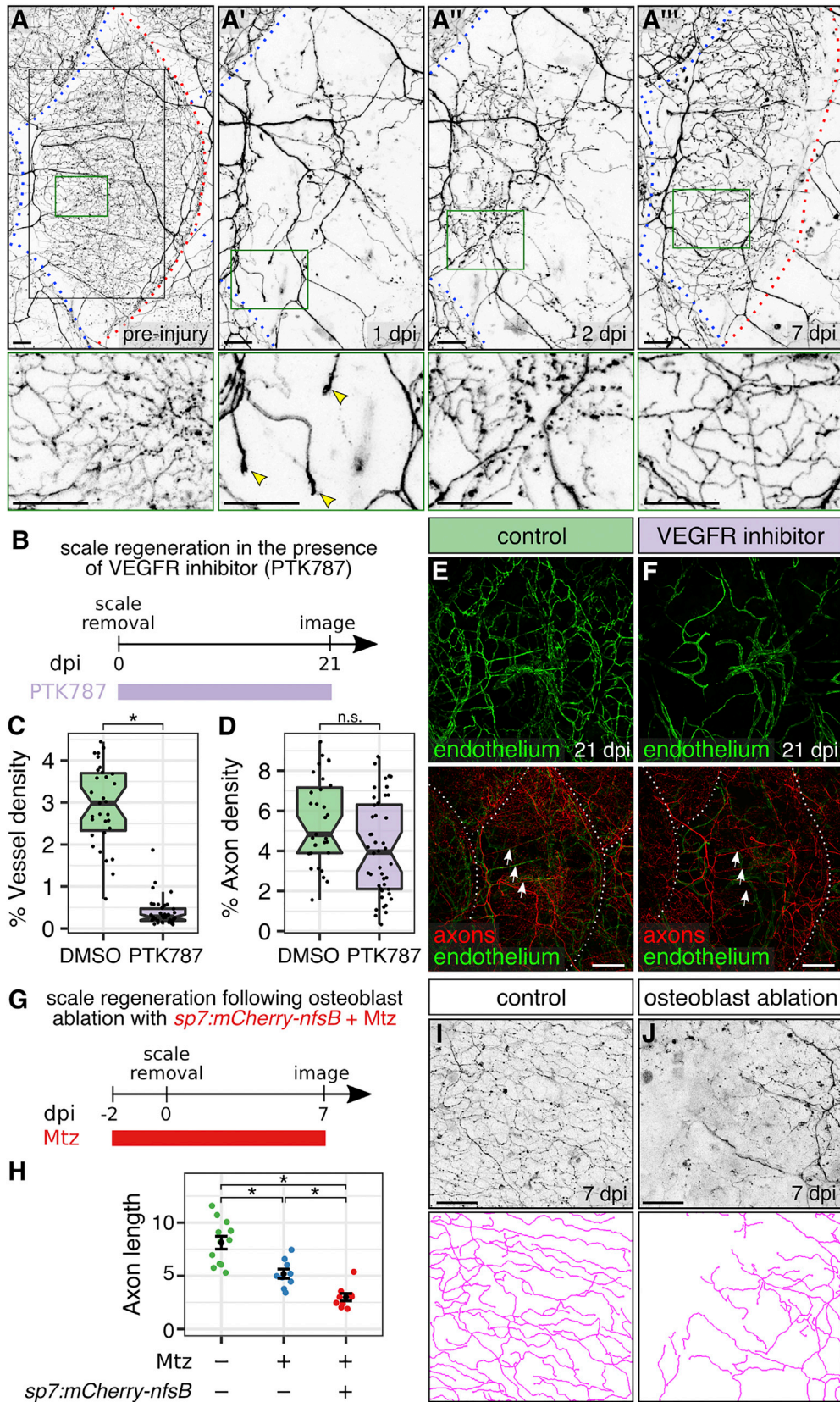
(I) Lateral views of nascent scales imaged from the anterior region of an intact animal at stage 10 mm SL (43 days post fertilization). Scales develop asynchronously from posterior to anterior (Sire et al., 1997a). Individual scales from adjacent regions of the body were cropped and ordered by size to create this composite. Note that radial osteoblasts first appear near the posterior scale margin (arrowheads).

(J) Schematic of scale transplant experiments.

(K and L) Widefield images of untransplanted control (K) and transplanted (L) scales showing sensory axons along a single radius. Images show overlays of the mCherry and DIC channels.

(M and N) Immunostaining of transplanted scales from donor fish of the indicated genotypes. Laminin staining marks the radii. Note growth of host axons along the donor radii.

Transgenes: (A) endothelium (*Tg(fli1a:EGFP)*) and axons (*Tg(p2rx3a:mCherry)*); (B) axons (*Tg(p2rx3b:EGFP)*), and keratinocytes and Schwann cells (*Tg(-28.5Sox10:Cre);Tg(actb2:BswitchR)*); (C) *Tg(p2rx3a>mCherry)*; (D) *Tg(sp7:mCherry-nfsB)*; (F) axons (*Tg(p2rx3b:EGFP)*), osteoblasts (*Tg(sp7:mCherry-nfsB)*), and keratinocytes (*Tg(actb2:BswitchR)*); (I) *Tg(sp7:mCherry-nfsB)*. Staining: (E) osteoblasts (zns-5), laminin (anti-laminin), and nuclei (DAPI); (G and H) osteoblasts (zns-5), axons (acTubulin), and nuclei (DAPI); (M and N) laminin (anti-laminin) and nuclei (DAPI). Scale bars, 25 μ m. See also Figures S5 and S6.



(legend on next page)

Osteoblasts Guide the Formation of a Bone-Associated Neurovascular Unit

Nerves are pioneered by axons that sense guidance cues laid out by other cells. Vasculature and nerves are often associated with and guide each other in vertebrates (Makita, 2013), but, in zebrafish, scales, nerves, and blood vessels form independently: nerves form before vasculature, but vasculature is unaffected by the absence of nerves. These observations suggest that other cells associated with scales lay down a path that guides nerves and endothelial cells separately. Indeed, we found that radial tracts in scales, built by osteoblasts, guide these cells. Since radii persist throughout life, they provide a mechanism not only for establishing the innervation pattern but also for re-establishing it when nerves are damaged and regenerate.

Peripheral nerves also interact with bony structures during development. For example, optic and cranial ganglia nerves, together with associated blood vessels, restrict skull ossification to create holes called foramina (Akbareian et al., 2015). In contrast to foramina development, in which nerves and blood vessels shape bones, we found that the mineralized pattern of bony scales determines the pattern of skin vascularization and innervation. Osteoblasts were the first cells we detected in a radial pattern. This observation suggests that osteoblasts either guide nerves and vessels or create an attractive environment for migration, perhaps by depositing a permissive ECM or concentrating guidance cues. Other bony appendages, such as antlers, tusks, and teeth, are also profusely innervated and vascularized (Hildebrand et al., 1995; Weissengruber et al., 2005; Wislocki and Singer, 1946). Thus, investigating mechanisms of bone-nerve interactions in scales could provide insight into the development of diverse appendages.

Scales Provide a Mechanism for Organizing Innervation of the Adult Skin

In larval flies, fish, and frogs, repulsive “tiling” interactions determine the arrangement of nociceptor innervation territories: sensory neurites grow until they are repelled by neighboring neurites (Frank and Westerfield, 1982; Grueber et al., 2002; Sagasti et al., 2005). Although the tiling process can explain how sensory neurites achieve comprehensive coverage of simple larval epithelia, it is not obvious how this mechanism could accommodate the addition of new neurons as the skin grows. Moreover, stratification of the skin into a multi-layered epithelium creates a three-dimensional innervation territory that presents a challenge to

tiling. An alternative method for achieving even innervation of the skin would be to use regularly spaced nerve conduits, each accommodating a fixed number of axons, to funnel axons into epidermal entry points.

Scales, usually thought of as a protective armature for fish, were not previously reported to associate with somatosensory nerves, but their structure provides an elegant solution to the spatial problem of distributing innervation. Since scales themselves are organized in a repeating pattern, and radii within them are evenly spaced, they provide a mechanism for creating regularly spaced skin entry points, and associating each with a vascular supply. Scales also polarize axons by transforming a primarily dorsal-ventral nerve trajectory into an anterior-posterior trajectory. A consequence of this nerve polarization is that free endings emerge toward the ends of nerves, allowing denser skin innervation at the edges of scales than at their bases. This property suggests that scale edges may be more sensitive to touch, similar to mammalian fingertips (Mancini et al., 2013).

The adult mammalian epidermis must also acquire even and comprehensive sensory innervation and the dermis must be vascularized. Although mammals do not have bony scales, it is possible that other patterned peripheral structures serve an analogous role in determining epidermal entry points and promoting angiogenesis. Scales are evolutionarily related to regularly spaced dermal appendages in other animal classes, like bird feathers and mammalian hair follicles, which all derive from dermal placodes and require ectodysplasin signaling (Aman et al., 2018; Harris et al., 2008; Kondo et al., 2001; Sadier et al., 2014). We speculate that these other dermal placodes, or the structures derived from them, may also pattern epidermal innervation and promote dermal vascularization.

STAR★METHODS

Detailed methods are provided in the online version of this paper and include the following:

- KEY RESOURCES TABLE
- CONTACT FOR REAGENT AND RESOURCE SHARING
- EXPERIMENTAL MODEL AND SUBJECT DETAILS
 - Zebrafish
- METHOD DETAILS

Figure 6. Osteoblasts, but Not Blood Vessels, Promote Epidermal Re-innervation following Injury

(A) Regeneration of a single scale and associated axons. Black box, region of images in (A')–(A''). Green boxes, regions of magnification in lower panels. Red dashed lines, scale margins before and after removal. Blue dashed lines, margins of non-injured scales. Note that regenerating axons developed growth cones in the dermis at 1 dpi (arrowheads), sparsely innervated the epidermis at 2 dpi, and more extensively innervated the epidermis at 7 dpi.

(B) Experimental design for scale regeneration in the presence of 500 nM PTK787.

(C and D) Boxplots of vessel (C) and axon (D) density based on *Tg(fli1a:EGFP)* expression or acTubulin staining, respectively, in regenerating scales at 21 dpi. $n = 31$ – 44 scales from $n = 2$ – 3 fish. * $p < 0.01$; n.s., not significant ($p > 0.01$); Wilcoxon rank-sum test.

(E and F) Representative lateral views of the indicated markers in control (DMSO) or VEGFR inhibitor (PTK787)-treated skin. Note that neither treatment prevented the formation or maintenance of nerves (arrows) over the course of the experiment. Dashed lines, scale margins.

(G) Timeline of osteoblast ablation using metronidazole (Mtz).

(H–J) Quantification (H) and representative lateral views and tracings (I and J) of regenerating axons in control or osteoblast-ablated fish (Mtz) at 7 dpi. Axon length is expressed as millimeters per 0.0625 mm^2 region of skin. $n = 9$ – 12 regions/treatment from $n = 2$ – 3 fish. Black bars, mean \pm SEM. * $p < 0.01$, Wilcoxon rank-sum test.

Transgenes: (A) axons (*Tg(p2rx3a>mCherry)*); (E and F) axons (*Tg(p2rx3a>mCherry)*) and endothelium (*Tg(fli1a:EGFP)*); (I and J) axons (*Tg(p2rx3b:EGFP)*). Scale bars, $50 \mu\text{m}$ (A, I, and J) and $200 \mu\text{m}$ (E and F). See also Figure S5.

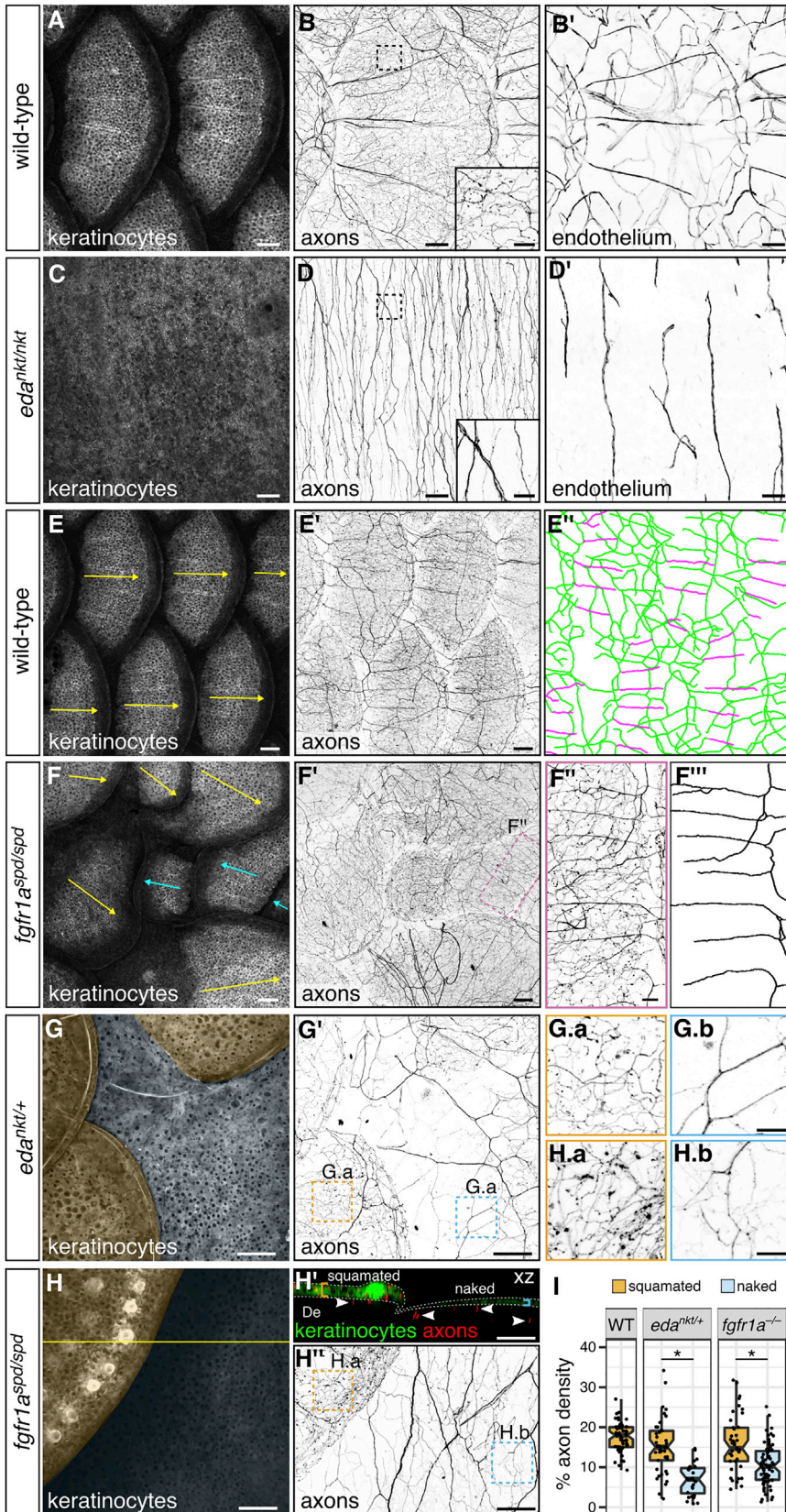


Figure 7. Scales Organize Epidermal Sensory Innervation and Vascularization

(A–D) Lateral views of wild-type and *eda*^{nkt/nkt} mutant skin. Note the absence of scales in *eda* mutants. Boxes, areas of magnification for insets in (B) and (D). Axons and vasculature below the hypodermis are obscured by pigmentation, causing them to appear unconnected.

(E and F) Lateral views of wild-type and *fgfr1a*^{spd/spd} mutant skin and associated tracings (E' and F'). Arrows, scale orientation. Blue arrows, posterior-anterior oriented scales. Note in (E') that nerves below scales (green) have a primarily dorsal-ventral orientation, whereas nerves above scales (magenta) have a primarily anterior-posterior orientation. Note reversed scale orientation (F) (blue arrows).

(G and H) Lateral and orthogonal views of skin from adults of the indicated genotypes. Orange and blue shading in (G) and (H) indicates squamated and naked skin, respectively. Arrowheads in (H') indicate axons in the dermis (De); brackets and dashed lines indicate epidermis. (G.a), (G.b), (H.a), and (H.b) are single z planes through the skin.

(I) Boxplots of axon density based on quantification of *Tg(p2rx3a>mCherry)* expression in squamated and naked skin from animals of the indicated genotypes. Quantification includes all axons within the field of view (dermis and epidermis). **p* < 0.01, Wilcoxon rank-sum test. *n* = 28–71 regions of 0.038–0.077 mm² were analyzed per category.

Transgenes: keratinocytes (*Tg(krt4:EGFP)*), axons (*Tg(p2rx3a>mCherry)*) and endothelium (*Tg(fli1a:EGFP)*). Scale bars, 100 μm (A–F', G, G', and H–H'') and 25 μm (insets in B and D; F'', G.a, G.b, H.a, and H.b). See also Figure S7.

- Mutant Identification
- Alizarin Red S Staining
- Scale Removal and Transplants
- Immunostaining
- Sectioning
- Electron Microscopy
- Osteoblast Ablation
- PTK787 Treatment
- Microscopy
- Live Imaging of Juveniles and Adults
- **QUANTIFICATION AND STATISTICAL ANALYSIS**
- Image Analysis and Statistics

SUPPLEMENTAL INFORMATION

Supplemental Information includes seven figures and can be found with this article online at <https://doi.org/10.1016/j.devcel.2018.06.019>.

ACKNOWLEDGMENTS

We thank Gage Crump, Shannon Fisher, Matthew Harris, Ellen Lien, Shuo Lin, David Parichy, Alex Schier, William Talbot, Ada Udvadia, Benoit Vanhollenbeke, Mark Voigt, and the Zebrafish International Resource Center (ZIRC) for generously sharing fish lines. We thank Michael Harrison and Sandeep Paul for helpful advice and discussions, Adam Langenbacher for vibratome training, Rick Klufas in the UCLA Life Sciences machine shop for the adult imaging chamber, Marianne Cilluffo in the UCLA Brain Research Institute for electron microscopy, and Stephen Basenfelder and Son Giang for fish care. We thank Samantha Butler and Ivan Duran for comments on the manuscript. This work was supported by a K99 award from NICHD to J.P.R. (K99HD086271) and a grant from NIAMS to A.S. (R01AR064582).

AUTHOR CONTRIBUTIONS

This study was conceived by J.P.R. and A.S. Most experiments were performed by J.P.R. with help from N.-T.V. J.P.R. analyzed the data and wrote the paper with help from A.S.

DECLARATION OF INTERESTS

The authors declare no competing interests.

Received: July 24, 2017

Revised: May 27, 2018

Accepted: June 22, 2018

Published: July 19, 2018

REFERENCES

- Akbareian, S.E., Pittsillides, A.A., Macharia, R.G., and McGonnell, I.M. (2015). Occipital foramina development involves localised regulation of mesenchyme proliferation and is independent of apoptosis. *J. Anat.* **226**, 560–574.
- Aman, A.J., Fulbright, A.N., and Parichy, D.M. (2018). Wnt/ β -catenin regulates an ancient signaling network during zebrafish scale development. *bioRxiv*. <https://doi.org/10.1101/293233>.
- Bayliss, P.E., Bellavance, K.L., Whitehead, G.G., Abrams, J.M., Aegerter, S., Robbins, H.S., Cowan, D.B., Keating, M.T., O'Reilly, T., Wood, J.M., et al. (2006). Chemical modulation of receptor signaling inhibits regenerative angiogenesis in adult zebrafish. *Nat. Chem. Biol.* **2**, 265–273.
- Bostaille, N., Gauquier, A., Stainier, D.Y.R., Raible, D.W., and Vanhollenbeke, B. (2017). Defective *adgra2* (*gpr124*) splicing and function in zebrafish ouchless mutants. *Development* **144**, 8–11.
- Braverman, I.M., and Yen, A. (1977). Ultrastructure of the human dermal microcirculation. II. The capillary loops of the dermal papillae. *J. Invest. Dermatol.* **68**, 44–52.
- Budi, E.H., Patterson, L.B., and Parichy, D.M. (2008). Embryonic requirements for ErbB signaling in neural crest development and adult pigment pattern formation. *Development* **135**, 2603–2614.
- Bussmann, J., Bos, F.L., Urasaki, A., Kawakami, K., Duckers, H.J., and Schulte-Merker, S. (2010). Arteries provide essential guidance cues for lymphatic endothelial cells in the zebrafish trunk. *Development* **137**, 2653–2657.
- Chatani, M., Takano, Y., and Kudo, A. (2011). Osteoclasts in bone modeling, as revealed by in vivo imaging, are essential for organogenesis in fish. *Dev. Biol.* **360**, 96–109.
- Chen, Z.-L., and Strickland, S. (2003). Laminin gamma1 is critical for Schwann cell differentiation, axon myelination, and regeneration in the peripheral nerve. *J. Cell Biol.* **163**, 889–899.
- Chen, S., Rio, C., Ji, R.-R., Dikkes, P., Coggeshall, R.E., Woolf, C.J., and Corfas, G. (2003). Disruption of ErbB receptor signaling in adult non-myelinating Schwann cells causes progressive sensory loss. *Nat. Neurosci.* **6**, 1186–1193.
- Cole, L.K., and Ross, L.S. (2001). Apoptosis in the developing zebrafish embryo. *Dev. Biol.* **240**, 123–142.
- Curado, S., Anderson, R.M., Jungblut, B., Mumm, J., Schroeter, E., and Stainier, D.Y.R. (2007). Conditional targeted cell ablation in zebrafish: a new tool for regeneration studies. *Dev. Dyn.* **236**, 1025–1035.
- Frank, E., and Westerfield, M. (1982). The formation of appropriate central and peripheral connexions by foreign sensory neurones of the bullfrog. *J. Physiol.* **324**, 495–505.
- Gau, P., Poon, J., Ufret-Vincenty, C., Snelson, C.D., Gordon, S.E., Raible, D.W., and Dhaka, A. (2013). The zebrafish ortholog of TRPV1 is required for heat-induced locomotion. *J. Neurosci.* **33**, 5249–5260.
- Grueber, W.B., and Sagasti, A. (2010). Self-avoidance and tiling: mechanisms of dendrite and axon spacing. *Cold Spring Harb. Perspect. Biol.* **2**, a001750.
- Grueber, W.B., Jan, L.Y., and Jan, Y.N. (2002). Tiling of the *Drosophila* epidermis by multidendritic sensory neurons. *Development* **129**, 2867–2878.
- Guzman, A., Ramos-Balderas, J.L., Carrillo-Rosas, S., and Maldonado, E. (2013). A stem cell proliferation burst forms new layers of P63 expressing suprabasal cells during zebrafish postembryonic epidermal development. *Biol. Open* **2**, 1179–1186.
- Hallmann, R., Horn, N., Selg, M., Wendler, O., Pausch, F., and Sorokin, L.M. (2005). Expression and function of laminins in the embryonic and mature vasculature. *Physiol. Rev.* **85**, 979–1000.
- Harris, M.P., Rohner, N., Schwarz, H., Perathoner, S., Konstantinidis, P., and Nüsslein-Volhard, C. (2008). Zebrafish *eda* and *edar* mutants reveal conserved and ancestral roles of ectodysplasin signaling in vertebrates. *PLoS Genet.* **4**, e1000206.
- Hildebrand, C., Fried, K., Tuisku, F., and Johansson, C.S. (1995). Teeth and tooth nerves. *Prog. Neurobiol.* **45**, 165–222.
- Honjo, Y., Kniss, J., and Eisen, J.S. (2008). Neuregulin-mediated ErbB3 signaling is required for formation of zebrafish dorsal root ganglion neurons. *Development* **135**, 2615–2625.
- Honjo, Y., Payne, L., and Eisen, J.S. (2011). Somatosensory mechanisms in zebrafish lacking dorsal root ganglia: somatosensory mechanisms in juvenile zebrafish. *J. Anat.* **218**, 271–276.
- Hughes, A. (1957). The development of the primary sensory system in *Xenopus laevis* (Daudin). *J. Anat.* **91**, 323–338.
- Humphrey, T. (1944). Primitive neurons in the embryonic human central nervous system. *J. Comp. Neurol.* **81**, 1–45.
- Humphrey, T. (1947). Sensory ganglion cells within the central canal of the embryonic human spinal cord. *J. Comp. Neurol.* **86**, 1–35.
- Humphrey, T. (1950). Intramedullary sensory ganglion cells in the roof plate area of the embryonic human spinal cord. *J. Comp. Neurol.* **92**, 333–399.
- van Impel, A., Zhao, Z., Hermkens, D.M.A., Roukens, M.G., Fischer, J.C., Peterson-Maduro, J., Duckers, H., Ober, E.A., Ingham, P.W., and Schulte-Merker, S. (2014). Divergence of zebrafish and mouse lymphatic cell fate specification pathways. *Development* **141**, 1228–1238.

- Jenkins, B.A., and Lumpkin, E.A. (2017). Developing a sense of touch. *Development* **144**, 4078–4090.
- Johnson, C.L., and Holbrook, K.A. (1989). Development of human embryonic and fetal dermal vasculature. *J. Invest. Dermatol.* **93**, 10S–17S.
- Johnson, S.L., and Weston, J.A. (1995). Temperature-sensitive mutations that cause stage-specific defects in Zebrafish fin regeneration. *Genetics* **141**, 1583–1595.
- Kague, E., Gallagher, M., Burke, S., Parsons, M., Franz-Odenaal, T., and Fisher, S. (2012). Skeletogenic fate of zebrafish cranial and trunk neural crest. *PLoS One* **7**, e47394.
- Kobayashi, I., Kobayashi-Sun, J., Kim, A.D., Pouget, C., Fujita, N., Suda, T., and Traver, D. (2014). Jam1a-Jam2a interactions regulate haematopoietic stem cell fate through Notch signalling. *Nature* **512**, 319–323.
- Kollros, J.J., and Bovbjerg, A.M. (1997). Growth and death of Rohon-Beard cells in *Rana pipiens* and *Ceratophrys ornata*. *J. Morphol.* **232**, 67–78.
- Kondo, S., Kuwahara, Y., Kondo, M., Naruse, K., Mitani, H., Wakamatsu, Y., Ozato, K., Asakawa, S., Shimizu, N., and Shima, A. (2001). The medaka rs-3 locus required for scale development encodes ectodysplasin-A receptor. *Curr. Biol.* **11**, 1202–1206.
- Kucenas, S., Soto, F., Cox, J.A., and Voigt, M.M. (2006). Selective labeling of central and peripheral sensory neurons in the developing zebrafish using P2X(3) receptor subunit transgenes. *Neuroscience* **138**, 641–652.
- Lamborghini, J.E. (1987). Disappearance of Rohon-Beard neurons from the spinal cord of larval *Xenopus laevis*. *J. Comp. Neurol.* **264**, 47–55.
- Lawson, N.D., and Weinstein, B.M. (2002). In vivo imaging of embryonic vascular development using transgenic zebrafish. *Dev. Biol.* **248**, 307–318.
- Lentz, S.I., Miner, J.H., Sanes, J.R., and Snider, W.D. (1997). Distribution of the ten known laminin chains in the pathways and targets of developing sensory axons. *J. Comp. Neurol.* **378**, 547–561.
- Lister, J.A., Robertson, C.P., Lepage, T., Johnson, S.L., and Raible, D.W. (1999). nacre encodes a zebrafish microphthalmia-related protein that regulates neural-crest-derived pigment cell fate. *Development* **126**, 3757–3767.
- Longair, M.H., Baker, D.A., and Armstrong, J.D. (2011). Simple neurite tracer: open source software for reconstruction, visualization and analysis of neuronal processes. *Bioinformatics* **27**, 2453–2454.
- Lyons, D.A., Pogoda, H.-M., Voas, M.G., Woods, I.G., Diamond, B., Nix, R., Arana, N., Jacobs, J., and Talbot, W.S. (2005). *erbb3* and *erbb2* are essential for Schwann cell migration and myelination in zebrafish. *Curr. Biol.* **15**, 513–524.
- Makita, T. (2013). Nerve control of blood vessel patterning. *Dev. Cell* **24**, 340–341.
- Malmquist, S.J., Abramsson, A., McGraw, H.F., Linbo, T.H., and Raible, D.W. (2013). Modulation of dorsal root ganglion development by ErbB signaling and the scaffold protein Sorbs3. *Development* **140**, 3986–3996.
- Mancini, F., Sambo, C.F., Ramirez, J.D., Bennett, D.L.H., Haggard, P., and Iannetti, G.D. (2013). A fovea for pain at the fingertips. *Curr. Biol.* **23**, 496–500.
- Metcalfe, W.K., Myers, P.Z., Trevarrow, B., Bass, M.B., and Kimmel, C.B. (1990). Primary neurons that express the L2/HNK-1 carbohydrate during early development in the zebrafish. *Development* **110**, 491–504.
- Mosimann, C., Kaufman, C.K., Li, P., Pugach, E.K., Tamplin, O.J., and Zon, L.I. (2011). Ubiquitous transgene expression and Cre-based recombination driven by the ubiquitin promoter in zebrafish. *Development* **138**, 169–177.
- Mukoyama, Y.-S., Shin, D., Britsch, S., Taniguchi, M., and Anderson, D.J. (2002). Sensory nerves determine the pattern of arterial differentiation and blood vessel branching in the skin. *Cell* **109**, 693–705.
- Munger, B.L., and Ide, C. (1988). The structure and function of cutaneous sensory receptors. *Arch. Histol. Cytol.* **51**, 1–34.
- Münzel, E.J., Schaefer, K., Oberei, B., Kremmer, E., Burton, E.A., Kuscha, V., Becker, C.G., Brösamle, C., Williams, A., and Becker, T. (2012). Claudin k is specifically expressed in cells that form myelin during development of the nervous system and regeneration of the optic nerve in adult zebrafish. *Glia* **60**, 253–270.
- Nencini, S., and Ivanusic, J.J. (2016). The physiology of bone pain. How much do we really know? *Front. Physiol.* **7**, 157.
- O'Brien, G.S., Rieger, S., Wang, F., Smolen, G.A., Gonzalez, R.E., Buchanan, J., and Sagasti, A. (2012). Coordinate development of skin cells and cutaneous sensory axons in zebrafish. *J. Comp. Neurol.* **520**, 816–831.
- Palanca, A.M.S., Lee, S.-L., Yee, L.E., Joe-Wong, C., Trinh, L.A., Hiroyasu, E., Husain, M., Fraser, S.E., Pellegrini, M., and Sagasti, A. (2013). New transgenic reporters identify somatosensory neuron subtypes in larval zebrafish. *Dev. Neurobiol.* **73**, 152–167.
- Pan, Y.A., Choy, M., Prober, D.A., and Schier, A.F. (2012). Robo2 determines subtype-specific axonal projections of trigeminal sensory neurons. *Development* **139**, 591–600.
- Parichy, D.M., Ransom, D.G., Paw, B., Zon, L.I., and Johnson, S.L. (2000). An orthologue of the kit-related gene *fms* is required for development of neural crest-derived xanthophores and a subpopulation of adult melanocytes in the zebrafish, *Danio rerio*. *Development* **127**, 3031–3044.
- Parichy, D.M., Elizondo, M.R., Mills, M.G., Gordon, T.N., and Engeszer, R.E. (2009). Normal table of postembryonic zebrafish development: staging by externally visible anatomy of the living fish. *Dev. Dyn.* **238**, 2975–3015.
- Patten, S.A., Sihra, R.K., Dhimi, K.S., Coutts, C.A., and Ali, D.W. (2007). Differential expression of PKC isoforms in developing zebrafish. *Int. J. Dev. Neurosci.* **25**, 155–164.
- Pittman, A.J., Law, M.-Y., and Chien, C.-B. (2008). Pathfinding in a large vertebrate axon tract: isotypic interactions guide retinotectal axons at multiple choice points. *Development* **135**, 2865–2871.
- Preibisch, S., Saalfeld, S., and Tomancak, P. (2009). Globally optimal stitching of tiled 3D microscopic image acquisitions. *Bioinformatics* **25**, 1463–1465.
- Rasmussen, J.P., Sack, G.S., Martin, S.M., and Sagasti, A. (2015). Vertebrate epidermal cells are broad-specificity phagocytes that clear sensory axon debris. *J. Neurosci.* **35**, 559–570.
- Reyes, R., Haendel, M., Grant, D., Melancon, E., and Eisen, J.S. (2004). Slow degeneration of zebrafish Rohon-Beard neurons during programmed cell death. *Dev. Dyn.* **229**, 30–41.
- Rezakhaniha, R., Ajianniotis, A., Schrauwen, J.T.C., Griffa, A., Sage, D., Bouten, C.V.C., van de Vosse, F.N., Unser, M., and Stergiopoulos, N. (2012). Experimental investigation of collagen waviness and orientation in the arterial adventitia using confocal laser scanning microscopy. *Biomech. Model. Mechanobiol.* **11**, 461–473.
- Riethmacher, D., Sonnenberg-Riethmacher, E., Brinkmann, V., Yamaai, T., Lewin, G.R., and Birchmeier, C. (1997). Severe neuropathies in mice with targeted mutations in the ErbB3 receptor. *Nature* **389**, 725–730.
- Rohner, N., Bercsényi, M., Orbán, L., Kolanczyk, M.E., Linke, D., Brand, M., Nüsslein-Volhard, C., and Harris, M.P. (2009). Duplication of *fgfr1* permits Fgf signaling to serve as a target for selection during domestication. *Curr. Biol.* **19**, 1642–1647.
- Sadier, A., Viriot, L., Pantalacci, S., and Laudet, V. (2014). The ectodysplasin pathway: from diseases to adaptations. *Trends Genet.* **30**, 24–31.
- Sagasti, A., Guido, M.R., Raible, D.W., and Schier, A.F. (2005). Repulsive interactions shape the morphologies and functional arrangement of zebrafish peripheral sensory arbors. *Curr. Biol.* **15**, 804–814.
- Schindelin, J., Arganda-Carreras, I., Frise, E., Kaynig, V., Longair, M., Pietzsch, T., Preibisch, S., Rueden, C., Saalfeld, S., Schmid, B., et al. (2012). Fiji: an open-source platform for biological-image analysis. *Nat. Methods* **9**, 676–682.
- Sharif, F., de Bakker, M.A.G., and Richardson, M.K. (2014). Osteoclast-like cells in early Zebrafish embryos. *Cell J.* **16**, 211–224.
- Singh, S.P., Holdway, J.E., and Poss, K.D. (2012). Regeneration of amputated zebrafish fin rays from de novo osteoblasts. *Dev. Cell* **22**, 879–886.
- Sire, J.-Y., and Akimenko, M.-A. (2004). Scale development in fish: a review, with description of sonic hedgehog (*shh*) expression in the zebrafish (*Danio rerio*). *Int. J. Dev. Biol.* **48**, 233–247.
- Sire, J.Y., Allizard, F., Babiar, O., Bourguignon, J., and Quilhac, A. (1997a). Scale development in zebrafish (*Danio rerio*). *J. Anat.* **190** (Pt 4), 545–561.

- Sire, J.-Y., Quilhac, A., Bourguignon, J., and Allizard, F. (1997b). Evidence for participation of the epidermis in the deposition of superficial layer of scales in zebrafish (*Danio rerio*): a SEM and TEM study. *J. Morphol.* *231*, 161–174.
- Slatter, C.A.B., Kanji, H., Coutts, C.A., and Ali, D.W. (2005). Expression of PKC in the developing zebrafish, *Danio rerio*. *J. Neurobiol.* *62*, 425–438.
- Svoboda, K.R., Linares, A.E., and Ribera, A.B. (2001). Activity regulates programmed cell death of zebrafish Rohon-Beard neurons. *Development* *128*, 3511–3520.
- Udvardi, A.J. (2008). 3.6 kb genomic sequence from Takifugu capable of promoting axon growth-associated gene expression in developing and regenerating zebrafish neurons. *Gene Expr. Patterns* *8*, 382–388.
- Vanhollebeke, B., Stone, O.A., Bostaille, N., Cho, C., Zhou, Y., Maquet, E., Gauquier, A., Cabochette, P., Fukuhara, S., Mochizuki, N., et al. (2015). Tip cell-specific requirement for an atypical Gpr124- and Reck-dependent Wnt/ β -catenin pathway during brain angiogenesis. *Elife* *4*, <https://doi.org/10.7554/eLife.06489>.
- de Vrieze, E., Sharif, F., Metz, J.R., Flik, G., and Richardson, M.K. (2011). Matrix metalloproteinases in osteoclasts of ontogenetic and regenerating zebrafish scales. *Bone* *48*, 704–712.
- Wang, F., Julien, D.P., and Sagasti, A. (2013). Journey to the skin: somatosensory peripheral axon guidance and morphogenesis. *Cell Adh. Migr.* *7*, 388–394.
- Waterman, R.E. (1970). Fine structure of scale development in the teleost, *Brachydanio rerio*. *Anat. Rec.* *168*, 361–379.
- Weis, J.S. (1968). Analysis of the development of nervous system of the zebrafish, *Brachydanio rerio*. I. The normal morphology and development of the spinal cord and ganglia of the zebrafish. *J. Embryol. Exp. Morphol.* *19*, 109–119.
- Weissengruber, G.E., Egerbacher, M., and Forstenpointner, G. (2005). Structure and innervation of the tusk pulp in the African elephant (*Loxodonta africana*). *J. Anat.* *206*, 387–393.
- Whitear, M. (1986). Epidermis. In *Biology of the Integument*, J. Bereiter-Hahn, A. Gedeon Matoltsy, and K. Sylvia Richards, eds. (Springer), pp. 8–38.
- Wiley, M.L., and Collette, B.B. (1970). Breeding tubercles and contact organs in fishes: their occurrence, structure, and significance. *Bull. Am. Mus. Nat. Hist.* *143*, article 3.
- Williams, J.A., Barrios, A., Gatchalian, C., Rubin, L., Wilson, S.W., and Holder, N. (2000). Programmed cell death in zebrafish rohon beard neurons is influenced by TrkC1/NT-3 signaling. *Dev. Biol.* *226*, 220–230.
- Wislocki, G.B., and Singer, M. (1946). The occurrence and function of nerves in the growing antlers of deer. *J. Comp. Neurol.* *85*, 1–19.
- Xu, C., Volkery, S., and Siekmann, A.F. (2015). Intubation-based anesthesia for long-term time-lapse imaging of adult zebrafish. *Nat. Protoc.* *10*, 2064–2073.
- Yaniv, S.P., and Schuldiner, O. (2016). A fly's view of neuronal remodeling. *Wiley Interdiscip. Rev. Dev. Biol.* *5*, 618–635.
- Youngstrom, K.A. (1944). Intramedullary sensory type ganglion cells in the spinal cord of human embryos. *J. Comp. Neurol.* *81*, 47–53.
- Yu, W.-M., Yu, H., Chen, Z.-L., and Strickland, S. (2009). Disruption of laminin in the peripheral nervous system impedes nonmyelinating Schwann cell development and impairs nociceptive sensory function. *Glia* *57*, 850–859.

STAR★METHODS

KEY RESOURCES TABLE

REAGENT or RESOURCE	SOURCE	IDENTIFIER
Antibodies		
Mouse monoclonal zns-5	Zebrafish International Resource Center	Cat# zns-5, RRID:AB_10013796
Mouse monoclonal zn-12	Zebrafish International Resource Center	Cat# zn-12, RRID:AB_10013761
Mouse anti-Tjp1 (ZO1-1A12)	Thermo Fisher Scientific	Cat# 33-9100, RRID:AB_2533147
Mouse anti-Acetylated Tubulin	Sigma-Aldrich	Cat# T6793, RRID:AB_477585
Rabbit anti-Laminin	Sigma-Aldrich	Cat# L9393, RRID:AB_477163
Rabbit anti-Acetylated Tubulin (Lys40) (D20G3)	Cell Signaling Technology	Cat# 5335S, RRID:AB_10544694
Chondroitin Sulfate Monoclonal Antibody (CS-56)	Thermo Fisher Scientific	Cat# MA1-83055, RRID:AB_929919
Goat Anti-Rabbit IgG H&L (Alexa Fluor 647) preadsorbed	Abcam	Cat# ab150087
Goat anti-Rabbit IgG (H+L) Cross-Adsorbed Secondary Antibody, Alexa Fluor 568	Thermo Fisher Scientific	Cat# A-11008, RRID:AB_143165
Goat anti-Rabbit IgG (H+L) Cross-Adsorbed Secondary Antibody, Alexa Fluor 568	Thermo Fisher Scientific	Cat# A-11011, RRID:AB_143157
Goat anti-Mouse IgG (H+L) Cross-Adsorbed Secondary Antibody, Alexa Fluor 488	Thermo Fisher Scientific	Cat# A-11001, RRID:AB_2534069
Goat anti-Mouse IgG (H+L) Cross-Adsorbed Secondary Antibody, Alexa Fluor 568	Thermo Fisher Scientific	Cat# A-11004, RRID:AB_2534072
Chemicals, Peptides, and Recombinant Proteins		
Tricaine-S (MS 222)	Western Chemical	CAS: 886-86-2
Metronidazole	Acros Organics	Cat# 210341000, CAS: 443-48-1
Alizarin Red S	Acros Organics	Cat# 400480250, CAS: 130-22-3
Vatalanib succinate (PTK787)	Toocris Bioscience	Cat# 5680, CAS: 212142-18-2
Alexa Fluor 488 Phalloidin	Thermo Fisher Scientific	Cat# A12379, RRID:AB_2315147
ProLong Gold Antifade Mountant	Thermo Fisher Scientific	Cat# P36930
Experimental Models: Organisms/Strains		
Zebrafish: AB (Wild-Type)	N/A	ZFIN: ZDB-GENO-960809-7
Zebrafish: <i>mitfa</i> ^{w2}	Lister et al., 1999	ZFIN: ZDB-ALT-990423-22
Zebrafish: <i>erb3b</i> ^{st48}	Lyons et al., 2005	ZFIN: ZDB-ALT-050512-6
Zebrafish: <i>adgr2</i> ^{sg84}	Vanhollebeke et al., 2015	ZFIN: ZDB-ALT-151020-1
Zebrafish: <i>fgfr1a</i> ^{t2227} (referred to as <i>fgfr1a</i> ^{spd})	Rohner et al., 2009	ZFIN: ZDB-ALT-100108-1
Zebrafish: <i>eda</i> ^{dt1261} (referred to as <i>eda</i> ^{nkt})	Harris et al., 2008	ZFIN: ZDB-ALT-090324-1
Zebrafish: <i>csf1ra</i> ^{j4blue}	Parichy et al., 2000	ZFIN: ZDB-ALT-001205-16
Zebrafish: <i>Tg(Tru.P2rx3a:LEXA-VP16,4xLEXOP-mCherry)</i> ^{la207} [referred to as <i>Tg(p2rx3a>mCherry)</i>]	Palanca et al., 2013	ZFIN: ZDB-TGCONSTRCT-130307-1
Zebrafish: <i>Tg(p2rx3b:EGFP)</i> ^{sl1}	Kucenas et al., 2006	ZFIN: ZDB-TGCONSTRCT-070117-110
Zebrafish: <i>TgBAC(trpa1b:EGFP)</i> ^{a129}	Pan et al., 2012	ZFIN: ZDB-TGCONSTRCT-120208-2
Zebrafish: <i>Tg(Tru.Gap43:EGFP)</i> ^{mil1}	Udvardia, 2008	ZFIN: ZDB-TGCONSTRCT-081120-1
Zebrafish: <i>Tg(-17.6isl2b:GFP)</i> ^{zc7}	Pittman et al., 2008	ZFIN: ZDB-TGCONSTRCT-100322-2
Zebrafish: <i>Tg(krt4:EGFP)</i> ^{la211}	Rasmussen et al., 2015	ZFIN: ZDB-TGCONSTRCT-150424-1
Zebrafish: <i>Tg(Mmu.Sox10-Mmu.Fos:Cre)</i> ^{zf384} [referred to as <i>Tg(-28.5Sox10:Cre)</i>]	Kague et al., 2012	ZFIN: ZDB-TGCONSTRCT-130614-2
Zebrafish: <i>Tg(actb2:LOXP-BFP-LOXP-DsRed)</i> ^{sd27} [referred to as <i>Tg(actb2:BswitchR)</i>]	Kobayashi et al., 2014	ZFIN: ZDB-TGCONSTRCT-141111-5

(Continued on next page)

Continued		
REAGENT or RESOURCE	SOURCE	IDENTIFIER
Zebrafish: <i>Tg(-3.5ubb:LOXP-EGFP-LOXP-mCherry)^{cz1701}</i> [referred to as <i>Tg(ubb:GswitchR)</i>]	Mosimann et al., 2011	ZFIN: ZDB-TGCONSTRCT-110124-1
Zebrafish: <i>Tg(cldnk:GAL4)^{ue101}</i>	Münzel et al., 2012	ZFIN: ZDB-TGCONSTRCT-120207-1
Zebrafish: <i>Tg(14xUAS:MA-GFP)^{ue102}</i>	Münzel et al., 2012	ZFIN: ZDB-TGCONSTRCT-120207-2
Zebrafish: <i>Tg(Ola.Sp7:mCherry-Eco.NfsB)^{pd46}</i> [referred to as <i>Tg(sp7:mCherry-nfsB)</i>]	Singh et al., 2012	ZFIN: ZDB-TGCONSTRCT-120503-4
Zebrafish: <i>Tg(fli1a:EGFP)^{y1}</i>	Lawson and Weinstein, 2002	ZFIN: ZDB-TGCONSTRCT-070117-94
Zebrafish: <i>TgBAC(prox1a:KALTA4,4xUAS-ADV.E1b:TagRFP)^{nims5}</i>	van Impel et al., 2014	ZFIN: ZDB-TGCONSTRCT-140521-2
Zebrafish: <i>Tg(-0.8ft1:RFP)^{hu5333}</i>	Bussmann et al., 2010	ZFIN: ZDB-TGCONSTRCT-110504-1
Oligonucleotides		
Primer: nkt-geno-forward: GTCGCTACAGTCACAACAGATG	This paper	N/A
Primer: nkt-geno-reverse: TTGGGGCTTTTAATGTTGCTGT	This paper	N/A
Primer: spd-geno-forward: GCAAATCTCTCAAATACACTGTGC	This paper	N/A
Primer: spd-geno-reverse: CAACTCTCACCAACAACACTAC	This paper	N/A
Primer: s984-geno-forward: GAACTGCAGACAAGCCATGA	This paper	N/A
Primer: s984-geno-reverse: TTCCCTTGGTAGGGTCACTG	This paper	N/A
Primer: ERB_01: GTGTCTGTTGCAGAATGGTAAA	Lyons et al., 2005	N/A
Primer: ERB_02: AGAAAACCCTGACTGGACCA	Lyons et al., 2005	N/A
Software and Algorithms		
Zen 2.1 (Blue edition)	Carl Zeiss Microscopy	http://www.zeiss.com
Fiji/ImageJ	Schindelin et al., 2012	https://fiji.sc/
R	R Foundation for Statistical Computing	https://www.r-project.org/

CONTACT FOR REAGENT AND RESOURCE SHARING

Further information and requests for resources and reagents should be directed to and will be fulfilled by the Lead Contact, Alvaro Sagasti (sagasti@mcdb.ucla.edu).

EXPERIMENTAL MODEL AND SUBJECT DETAILS

Zebrafish

Zebrafish (*Danio rerio*) were grown at 28.5°C on a 14 h/10 h light/dark cycle. See [Key Resources Table](#) for mutant and transgenic strains used. Zebrafish of both sexes were used in this study. Animals were staged according to standard length (Parichy et al., 2009). Unless stated otherwise, adult fish were between 18.5-30 mm SL and 3-12 months old. All experimental procedures were approved by the Chancellor's Animal Research Care Committee at UCLA.

METHOD DETAILS

Mutant Identification

Heterozygous carriers of the *nkt*, *spd*, *s984* and *st48* alleles were identified by restriction fragment length polymorphism using the restriction enzymes XbaI, AclI, HpyCH4III and Hpy166II, respectively, and the oligonucleotides listed in the [Key Resources Table](#). Homozygous mutants were identified by scale defects (*nkt*, *spd*) (Harris et al., 2008; Rohner et al., 2009), pigment defects (*st48*, *j4blue*, *adgra2*) (Budi et al., 2008; Parichy et al., 2000; Vanhollebeke et al., 2015) or loss of larval DRGs, as judged by *Tg(-17.6isl2b:GFP)* expression (*st48*, *s984*) (Honjo et al., 2008; Vanhollebeke et al., 2015). In our analysis of *erbb3b^{-/-}* mutants, we only analyzed scales in which we verified that there was no innervation, as judged by the absence of expression from a neuronal transgenic line or staining for acetylated tubulin.

Alizarin Red S Staining

To visualize mineralized bone, live animals were stained in 0.01% (wt/vol) alizarin red S (ACROS Organics), dissolved in system water for 15 minutes, and rinsed 3x5 minutes in system water.

Scale Removal and Transplants

To remove scales, fish were first anesthetized in 0.016% (wt/vol) MS-222 (Western Chemical) dissolved in system water. Scales were removed by seizing their posterior region with fine forceps, then pulling them backward. Scales were usually removed from the lateral trunk region anterior to the dorsal fin. Fish were recovered by flushing the gills with system water until opercular movement resumed.

Scale transplants were performed by removing one or two scales from the lateral trunk of *nacre; Tg(p2rx3a>mCherry)* fish, which lack melanophores. Donor scales were chosen from the dorsolateral trunk region, where scales contain melanophores, and moved into the empty host scale pocket. The difference in pigmentation distinguished the donor scale from host scales.

Immunostaining

Isolated scales were fixed in 4% PFA/PBS for 10–20 minutes at room temperature. Scales were washed 3x5 min in 0.1% Triton X-100 in PBS (PBST), then incubated overnight at 4°C with the appropriate primary antibody (see [Key Resources Table](#) for antibodies used) diluted in PBST. Scales were washed 4x15 min in PBST then incubated for 2 h at room temperature with the appropriate secondary antibody diluted 1:500 in PBST, followed by 4x15 min washes in PBST. To visualize nuclei, scales were incubated for 5 min in 5 ng/μl DAPI in PBS, followed by 4x5 min washes in PBST. Phalloidin staining was performed according to the manufacturer. Scales were mounted in a drop of ProLong Gold antifade mountant that was placed inside reinforcement label (Avery 5722) attached to a microscope slide. Coverslips were sealed with nail polish.

Sectioning

1–1.5 cm pieces of fish trunk were fixed in 4% PFA/PBS for 24h at room-temperature, washed 3x5 minutes in PBS, embedded in 4% (wt/vol) agarose and cut into 200 μm thick sections using a Vibratome 100 plus.

Electron Microscopy

Isolated scales were prepared for TEM as described ([Sire et al., 1997b](#)), with the following modifications: after dehydration, scales were treated with propylene oxide (PO), infiltrated with PO:Eponate 12, and embedded in Eponate 12. Semithin sections (0.2 μm) stained with toluidine blue were used for orientation. Thin sections (50 nm) were placed on Formvar coated copper slot grids, stained with saturated uranyl acetate and Reynolds' lead citrate, and examined on a JEOL 100CX at 60kV.

Osteoblast Ablation

To ablate osteoblasts, *Tg(sp7:mCherry-nfsB)* fish were treated nightly for 16h in the dark with 7 mM metronidazole (ACROS Organics) dissolved in system water. Controls were treated with system water alone. Treated fish were returned to tanks each morning and maintained on a normal feeding cycle for the course of treatment. Scale regeneration was induced by removing 8–10 scales from each of two adjacent dorsolateral rows of scales from the anterior trunk.

PTK787 Treatment

The VEGFR inhibitor PTK787 (Tocris Bioscience) was dissolved in DMSO to a stock concentration of 50 mM. To prevent angiogenesis, fish were treated with 500 nM PTK787 diluted in system water, as previously described ([Bayliss et al., 2006](#)). Controls were treated with 0.00001% DMSO diluted in system water. Fish were maintained in tanks with non-circulating water, which was replenished every 2–3 days. Scale regeneration was induced by removing 8–10 scales from each of two adjacent dorsolateral rows of scales from the anterior trunk.

Microscopy

Confocal imaging was performed on an LSM 510 or 800 confocal microscope (Carl Zeiss). Widefield imaging was performed on an Axioskop 2 or a SteREO Discovery.V12 (Carl Zeiss).

Live Imaging of Juveniles and Adults

Imaging of living zebrafish was performed using a custom intubation apparatus, modeled on a previously described method ([Xu et al., 2015](#)). Fish were anesthetized using 0.016% MS-222 until opercular movement ceased. Anesthetized fish were mounted in a custom-built Perspex imaging chamber and partially embedded in 1% agarose dissolved in system water, with gills, mouth and lateral trunk exposed. Fish were intubated with polyethylene tubing (Becton Dickinson #427421 or #427400) and freshly prepared MS-222 (0.006%–0.012%) was flowed at a rate of 1–6 ml/min through the mouth using an RP-1 peristaltic pump (Rainin). Fish were anesthetized for 1–2 h and recovered by intubation with system water.

QUANTIFICATION AND STATISTICAL ANALYSIS

Image Analysis and Statistics

Confocal image stacks were z-projected (maximum intensity projection), and brightness and contrast enhanced in Fiji (Schindelin et al., 2012). Tiled images were stitched using either the Pairwise Stitching or Grid/Collection Stitching plugins (Preibisch et al., 2009). Axon and blood vessel density analysis was performed by thresholding the appropriate channel; thresholds were applied uniformly between conditions. For isolated scales, a region of interest (ROI) was traced around the epidermis, using the DAPI or phalloidin channels as a reference. For intact adults, several ROI per field of view were typically used. In both cases, the 'area fraction' measurement was used to determine the fraction of non-zero pixels within the ROI. The Simple Neurite Tracer plugin (Longair et al., 2011) was used to trace axons. The OrientationJ plugin (Rezakhaniha et al., 2012) was used to analyze axon and blood vessel orientation. R (<https://www.r-project.org/>) was used to generate plots and perform statistical tests. Statistical details for each experiment are reported in the figure and figure legends. Significance is defined as a p-value less than 0.01, as indicated by the statistical method reported for each experiment.